SLAC-PUB-1982
July 1977

QUARK DYNAMICS AND PARTICLE PRODUCTION IN HIGH ENERGY COLLISIONS*

Stanley J. Brodsky

Stanford Linear Accelerator Center
Stanford University, Stanford, California 94305

Abstract: We discuss three problems relating to the basic interactions of quarks, gluons, and hadrons: (1) jet production and the dynamical role of color, (2) large transverse momentum phenomena, and (3) particle production on a nuclear target.

(Lectures given at the International Symposium on Hadron Structure and Multiparticle Production, Kazimierz Dolny, May 24-27, 1977.)

*Work supported by the Energy Research and Development Administration.

PREFACE

In these three lectures, we consider the phenomenological implications for hadron dynamics which derive from an underlying quark-gluon theory. In the first lecture we discuss the possible quantitative connections between initial color separation and the number of particles produced in a high energy collision. We also discuss how multiparticle jets which originate from quarks, multiquarks, hadrons, or gluons can be discriminated. A possible two component quark/exchange, gluon/exchange mechanism for Pomeron physics is also discussed. Various mechanisms for gluon jet production are also considered. The work in this lecture is based on several collaborations with R. Blankenbecler, W. Caswell, J. Gunion, R. Horgan, and N. Weiss.

In the second section, written in collaboration with R. Blankenbecler and J. Gunion, large transverse momentum processes are discussed within the framework of the constituent interchange model. The predictions of the constituent interchange model are found to be consistent with the normalization, as well as the scaling laws and angular dependence, of measured large p_T meson and baryon cross sections. The normalization of the hadronic couplings to valence quarks is computed. Predictions for quantum number correlations between the trigger particles and away side jets are discussed. We also contrast the predictions of the CIM and quark-quark scattering models.

A final version of this work taking into account more realistic parametrization of the structure functions, etc. will be published elsewhere.

In the third lecture we consider hadron-nucleus and nucleus-nucleus collisions from the standpoint of a rather standard quark-parton model. We predict that shadowing should be absent in the scaling region of deep inelastic scattering at large q^2 independent of x_{Bj}. Though extremely simple, the model is consistent with Glauber theory, and its predictions for hadron multiparticles and particle distributions in nuclear collision appear to be in excellent agreement with experiment. This work was done in collaboration with J. F. Gunion, and J. H. Kühn.

(A) JET PRODUCTION AND THE DYNAMICAL ROLE OF COLOR

I. Introduction

The production of multiparticle jets appears to be a common feature of all high energy hadron- and lepton-induced reactions.[1] Despite the indications that their average multiplicity[2] $\langle n \rangle$ and transverse momentum distributions are surprisingly similar, the underlying quark and gluon content of these jets can be quite diverse. In particular, we expect quark fragmentation jets of various flavors in $e^+e^- \to$ hadrons, as well as in the current fragmentation region of lepton-induced reactions. We also expect di-quark (qq) and multiquark jets in the target fragmentation region in deep inelastic scattering as well as in the beam and target region in Drell-Yan massive pair production. In the case of large p_T reactions, one expects quark, multiquark, and even jets of hadronic parentage depending on the hard scattering subprocess. Even more intriguing, if one takes quantum chromodynamics at face value, one must expect at some level, the production of jets corresponding to gluon fragmentation in any of these processes. In the case of ordinary forward hadronic reactions, the jet-like forward and backward multiparticle systems are usually considered to have a conventional hadronic origin, but as we shall discuss in Sections VI and VII, the primary parents of these systems could well be colored, if the initial hadronic interaction can be identified as being due to gluon or quark exchange.

One of the important phenomenological questions in particle physics, then, is how to empirically discriminate between jets of different origin, i.e., how to distinguish the different flavor, color, number of quarks or gluons of their parent systems. In this paper I will discuss a number of discriminants, including dn/dy (the height of the rapidity plateau in the central region) (Section VII), the fragmentation properties (the power-law falloff and quantum numbers of leading particles at $x \to 1$) (Section IV), and the possible retention of charge and other quantum numbers (Section II). The multiquark jet which is left behind in the target fragmentation region in deep inelastic scattering and the Drell-Yan process is especially interesting because of theoretical uncertainties regarding the composition of the hadron's parton wavefunction. We discuss special tests for such systems in Section II. Finally, in Section VII we speculate on the possibility that the initial color separation controls the height of the multiplicity plateau, and that events with large multiplicities are sensitive to gluon exchange contributions.

II. Charge Retention by Quark and Multiquark Systems[3]

Feynman[4] originally proposed the elegant ansatz that the total charge of a jet

$$<Q>_J = \sum_{h \epsilon J} Q_h \int_0^1 \frac{dn_{h/J}}{dx} dx = \sum_{h \epsilon J} Q_h \int_{y_0}^{y_{max}} \frac{dn_{h/J}}{dy} dy \tag{2.1}$$

could reflect, in the mean, the charge of its parent. However, as noted by Farrar and Rosner,[5] this connection can fail in specific model calculations, and accordingly there has been little subsequent interest in using this method as a jet discriminant.

In order to see why exact charge retention fails, consider the simple model for $e^+e^- \to \gamma \to q\bar{q} \to$ hadrons shown in Fig. 1. The rapidity interval $|y| < y_{max} \sim \frac{1}{2} \log s$ is filled uniformly by the production of neutral gluons, which subsequently decay to $q\bar{q}$ pairs. These then recombine with the leading quarks to produce mesons. If we could cut through a

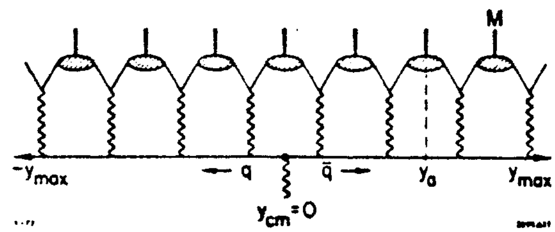

Fig. 1. Simplified model for the rapidity distribution of virtual gluons and mesons in $e^+e^- \to q\bar{q} \to$ hadrons. See also Section III.

meson and sum all the charges to the right of the point y_a, then clearly $Q_J(y > y_a) = Q_{\bar{q}}$. However, since we must sum over hadron charges an extra quark is always included in the sum, and the total charge corresponding to the antiquark jet is[3,5]

$$<Q>_J = Q_{\bar{q}} + \eta_Q \tag{2.2}$$

where $\eta_Q = <Q_q>_{sea}$ is the mean charge of quarks in the sea: $\eta_Q = \frac{1}{2}(2/3 - 1/3) = 1/6$ for an SU(2)- (or SU(4)-) symmetric sea, and $\eta_Q = \frac{1}{3}(2/3 - 1/3 - 1/3) = 0$ for an SU(3)-symmetric sea. Actually this result is quite model-independent, and Eq. (2.2) will apply to all jets which need a quark for neutralization. More generally, for any conserved charge $\Lambda = I_Z$, B, S, etc., one predicts[3,5]

$$<\Lambda>_J = \Lambda_J \pm \eta_\Lambda \tag{2.3}$$

where Λ_J is the quantum number of the parent quark or multiquark system and the sign is + (-) if the parent needs a quark (antiquark) to neutralize it. Notice that η_Λ is independent of the process and of the jet type and is a <u>universal number</u>.[3] The result (2.3) is unaffected by resonance decay or baryon production. From parametrizations[6] of the quark

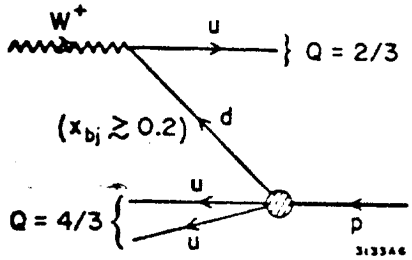

Fig. 2. Parton model diagram for $\nu p \to \mu^- X$ as viewed in the W^+p c.m. system for the valence region ($x_{bj} \gtrsim 0.2$).

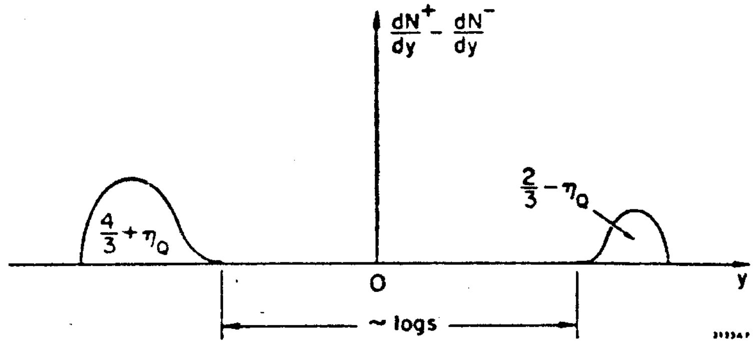

Fig. 3. Idealized distribution for $W^+p \to X$ ($\nu p \to \mu^- X$) as $s \to \infty$.

distribution functions, one can already determine empirically that $\eta_Q \cong 0.07$, corresponding to partial suppression of the strange and heavy quarks in the sea. For the usual quark models, $\eta_B = \frac{1}{3}$, $\eta_{I_Z} = 0$.

Given the fact that the η_Λ are universal numbers which can be established empirically, quantum number retention can be a viable method for identifying specific quark and multiquark systems. For example, Fig. 2 shows the expected initial quark flow in the W^+p c.m. system for $\nu p \to \mu^- X$, in the valence quark region $x_{bj} \gtrsim 0.2$, and Fig. 3 indicates the predicted hadronic charge distribution $dN^+/dy - dN^-/dy$ expected at very large $s = (q+p)^2$. For $x_{bj} < 0.2$, the presence of sea quarks which can be hit by the W^+ tends to further increase the asymmetry between the two hemispheres. Taking

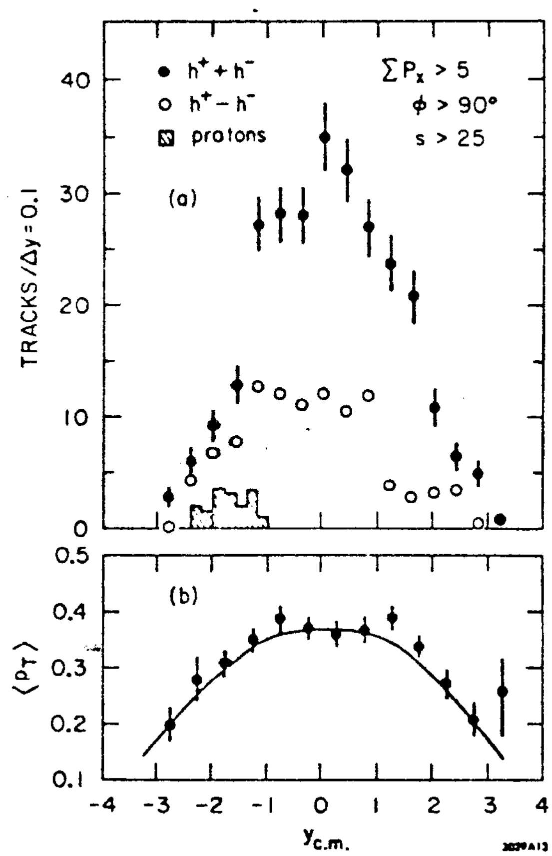

Fig. 4. Data from the Fermilab 15 ft bubble chamber for $\nu p \to \mu^+ X$.[7] The rapidity distribution and the charge structure $dN^+/dy - dN^-/dy$ of the final state are shown, as well as the transverse momentum distribution of the emitted hadrons. The curve for $\langle p_T(y) \rangle$ is from pp reactions.

$\eta_Q = 0.07$, this implies that the plateau height will be $\gtrsim 2.3$ times larger in the target (uu) fragmentation region compared to the current (u) fragmentation region. The data[7] (Fig. 4a)

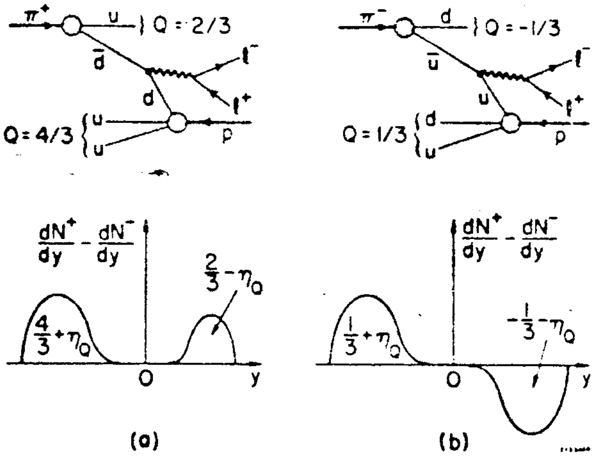

Fig. 5. The Drell-Yan mechanism and the expected charge distribution for $\pi^{\pm}p \rightarrow \ell^+\ell^- + X$ in the valence-valence region (x_π, $x_p \gtrsim 0.2$).

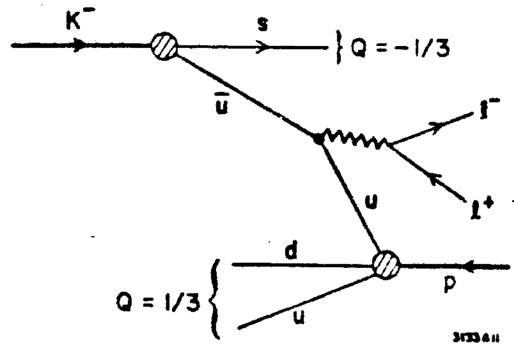

Fig. 6. The Drell-Yan mechanism for $K^-p \rightarrow \ell^+\ell^- + X$ in the valence-valence region (x_K, $x_p \gtrsim 0.2$).

seem consistent with this prediction. It is also interesting to note that the transverse momentum distribution of W^+-induced events is the same as that measured in pp collisions, shown by the solid lines in Fig. 4b.

One of the most interesting areas of application of the charge retention technique is to confirm the underlying quark structure predicted by the Drell-Yan process.[8] For example consider $\pi^{\pm}p \rightarrow \ell^+\ell^- X$ in the valence quark region (x_a, $x_b \gtrsim 0.2$; $x_a - x_b \cong x_L$, $x_a x_b \cong \mathcal{M}^2/s$). The predicted quark-flow diagrams and the charge distribution of the final state hadrons are shown in Fig. 5. We estimate that the width of the charged fragmentation regions is ~2-3 units in rapidity so very large s is needed to make a clear separation. Even at moderate s, though, one can study the ratio of the charge-difference plateau heights.

Because of the high energies available, and the possibility of controlling the momentum fractions x_a and x_b, systematic measurements of the hadron fragmentation region in the Drell-Yan process can lead to essential information on the complete hadron wavefunction in both the wee and valence quark domain. For example, the expected charge distribution in the valence region for $K^-p \rightarrow \ell^+\ell^- X$ is shown in Figs. 6 and 7. As in the previous examples, we assume that the (uud) Fock space wavefunction is the dominant component in the proton at large x_{bj}, and that the rapidities of the spectator u and d quarks are nearly equal to the initial rapidity. If we now consider events with x_b small

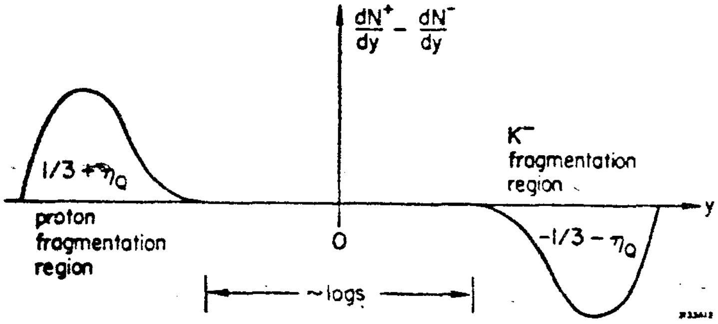

Fig. 7. The expected distribution of charge in rapidity for the process of Fig. 6.

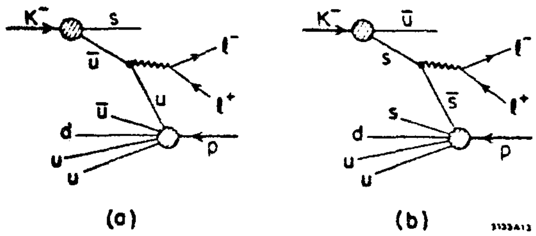

Fig. 8. The Drell-Yan mechanism for $K^-p \to \ell^+\ell^-X$ in the "valence-sea" region $(x_K \gtrsim 0.2,\ x_p \lesssim 0.2)$.

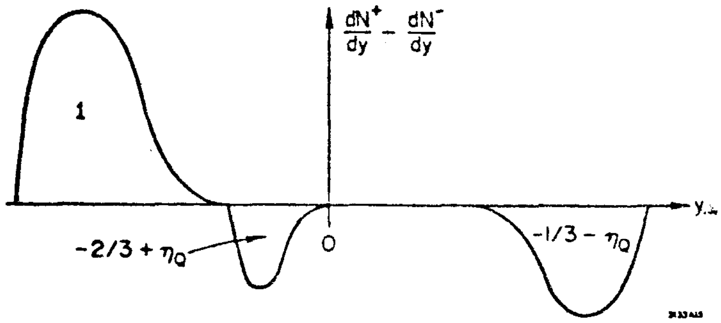

Fig. 9. The expected distribution of charge in rapidity for the process of Fig. 6 in the "hole fragmentation" model.

or wee, diagrams 8a and 8b become important (with a dominant because $Q_u^2 = 4Q_s^2$). In models where the extra $u\bar{u}$ pair is created from a neutral system, e.g., from gluon decay as in Ref. 9, then the wee quark charge is compensated locally in rapidity, and one expects the charge distribution shown in Fig. 9. This is also the prediction of the "hole" fragmentation model of Bjorken[10] and Feynman.[4] On the other hand, the charge distribution of the proton fragments may be more homogeneous, since it is possible that the interacting wee quarks are constituents of virtual charged and neutral mesons, as suggested in Ref. 11. The same result is predicted if we assume that the bound quarks of the spectator system exchange momentum and tend to equalize their velocities.[12] The resulting charge distribution would thus resemble Fig. 10. Thus detailed measurements of the charge flow in the hadron fragmentation regions could well distinguish between these basic theoretical models. Comparison between the Drell-Yan process, ψ production, and ordinary collisions should be illuminating.

Other tests of charge and quantum number retention, especially in e^+e^- annihilation, are discussed in Ref. 3.

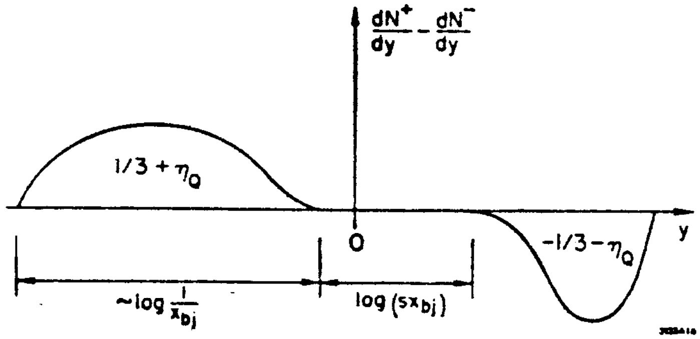

Fig. 10. An alternate possibility for the distribution of charge in rapidity for the process of Fig. 8.

III. A Model for Jet Fragmentation[3]

One of the basic uncertainties in the quark model is the nature of the space-time evolution of the final state hadrons. In constructing a model one must keep in mind that (aside from resonance decay) the emission of one hadron cannot cause nor directly influence the emission of other hadrons, since they are at a space-like separation. A simple model for $e^+e^- \to$ hadrons, which is a realization of Bjorken's inside-outside cascade mechanism,[10] is shown in Fig. 11. After the $q\bar{q}$ begin to separate, (virtual) gluons are emitted with flat distribution in rapidity. One assumes that each gluon lives, on the average, a characteristic proper time $\tau = 1/d$, producing quarks and antiquarks which recombine to form color singlet mesons. The hadron production then occurs near the hyperboloid, $t^2 - x^2 = d^2$, which meets the quark world line at $t \sim \gamma d$. The initial quark and antiquark are thus free for a time $t \propto \sqrt{s}$ which justifies them as being treated as free particles in the calculation of the annihilation cross section. In the e^+e^- center-of-mass frame, the fastest mesons are emitted last.[13]

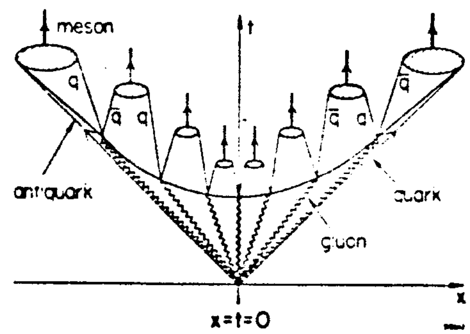

Fig. 11. Space-time evolution of the hadronic final state in e^+e^- annihilation. The initial $q\bar{q}$ pair is produced at $x=t=0$ and the hadrons are produced near the hyperboloid, $t^2 - x^2 = d^2$. The transverse direction is not shown in the diagram.

Although this model is grossly oversimplified, it is causal and covariant and has many characteristics expected in gauge theories and jet production. Resonance and baryon production can also be included. The model can serve as a simple testing ground for the effects of quark mass and valence effects, etc. An application is the quantum number retention rule, Eq. (2.3). Further, in this simple model the meson multiplicity is roughly equal to the gluon multiplicity and grows logarithmically. We discuss this feature further in the color model of Section VI.

IV. Leading Particle Behavior

In addition to its retained quantum numbers an important discriminant of a jet is the $x \to 1$ behavior of its leading particles. The basic idea is as follows: consider a fast moving composite system A with a large momentum $\vec{p}_A // z$. See Fig. 12a. The probability that one constituent (or subset of constituents) a, in a virtual state, has nearly all the momentum of A must vanish rapidly as the remaining constituents, the $n(\bar{a}A)$ spectators, are forced to low momentum. In fact, assuming an underlying scale-invariant model one finds[14]

$$G_{a/A}(x) = \frac{dN_{a/A}(x)}{dx} \underset{(x \to 1)}{\longrightarrow} C(1-x)^{2n(\bar{a}A)-1} \tag{4.1}$$

where x is the light cone momentum fraction, $x = \left(p_0^a + p_z^a\right) / \left(p_0^A + p_z^A\right)$. This result for the probability distribution leads to the predictions $\nu W_{2p} \sim G_{q/p}(x) \sim (1-x)^3$, $\nu W_{2\pi} \sim (1-x)$, $G_{\pi/q} \sim (1-x)$, $G_{\bar{q}/p} \sim (1-x)^7$, $G_{M/B} \sim (1-x)^5$, etc. Comparisons with experiment, corrections and other modifications are discussed in Ref. 1.

An immediate application of the counting rule (4.1) is the prediction of the $x_L = p_z^{c.m.} / p_{z\,max}^{c.m.}$ dependence of the forward inclusive cross section for the dissociation of a composite system. For example, one predicts for fast nuclear collisions (see Fig. 12b)

$$\frac{1}{\sigma} \frac{d\sigma}{dx_L}(A + B \to p + X) \sim (1-x_L)^{6(A-1)-1} \tag{4.2}$$

and

$$\frac{1}{\sigma} \frac{d\sigma}{dx_L}(A + B \to A' + X) \sim (1-x_L)^{6(A-A')-1} \tag{4.3}$$

since there are 3(A-A') quark spectators forced to low momentum. These and other predictions have recently been shown in a beautiful analysis by Schmidt and Blankenbecler[15] to be in striking

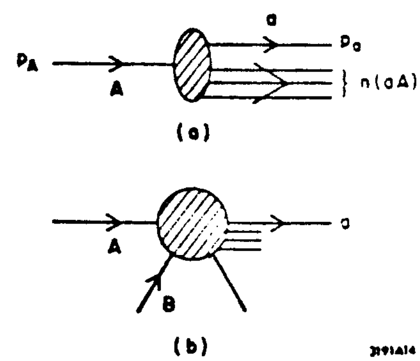

Fig. 12. (a) Fragmentation of A into a subset of constituent a. The number of elementary constituent spectators is $n(\bar{a}A)$. (b) Fragmentation of $A + B \to a + X$.

agreement with measurements of deuteron, alpha, and carbon dissociation at LBL. The prediction $G_{p/d} \sim (1-x)^5$ is also consistent with the Fermi motion observed in measurements of $ed \to epn$ for $x = -q^2/2p_d \cdot q \sim 1$.[16]

One of the most intriguing applications[17] of the counting rule (4.1) is to forward inclusive hadron reactions $pp \to \pi X$, etc. For $x_L \to 1$ this is normally considered the domain of the triple Regge mechanism, where $d\sigma/dx\,(A+B \to C+X) \sim (1-x)^{1-2\alpha(t)}$. However, in the range $0.2 < x_L < 0.8$ the measured cross sections[18] appear to have p_T-independent powers of $(1-x)$ (especially when parametrized in terms of $x_R = p^{c.m.}/p^{c.m.}_{max}$ and is thus more suggestive of a fragmentation mechanism.

At this point we shall distinguish three possible fragmentation models for high energy hadron collisions[19]:

(1) The incoming beam is dissociated by the Pomeron.[17] Then as in Eq. (4.1) $d\sigma/dx\,(A+B \to C+X) \sim (1-x_C)^{2n(\bar{C}A)-1}$; i.e., the fragmenting jet is the excited hadron A. (Although x_C is defined as the light-cone variable, $x_C = x_R$ should be sufficiently accurate.)

(2) Inelastic collisions begin with the exchange of a color gluon, as in the Low[20]-Nussinov[21] model. See Fig. 15e'. The fragmenting jet is then an octet $(A)_8$ with the same quark structure as A. Again, one predicts the same distribution as in (1), if $C \neq A$.

(3) Inelastic collisions begin with the exchange (or annihilation) of a wee quark, as in the Feynman wee parton model, as in Fig. 15e. The fragmenting jet then has one fewer spectator compared to the gluon or dissociation mechanisms. We thus have[19]

$$d\sigma/dx\,(A+B \to C+X) \sim (1-x_C)^{2n(\bar{C}A)-3} \tag{4.4}$$

For example, for $pp \to \pi^+ X$, the π^+ can be formed from the five-quark $|duu\bar{d}d\rangle$ Fock-state component of the proton. The Pomeron or gluon excitation models (1) and (2) then give $d\sigma/dx \sim (1-x)^5$, corresponding to three spectators (dud), whereas wee quark exchange (3) gives $d\sigma/dx \sim (1-x)^3$. The ISR data[18] for $pp \to \pi^+ X$ is consistent with $(1-x_\pi)^{3.1}$ for $p_T < 0.85$ GeV, $0.4 < x < 0.9$ when fit using the variable $x_R = p^{c.m.}/p^{c.m.}_{max}$, or $(1-x_L)^{3.5}$ when fit using $x_L = p_z^{c.m.}/p^{c.m.}_{z\,max}$. This then gives support to the quark exchange picture. We discuss further consequences of this model for hadron multiplicities in Sections VI and VII.

Predictions for particle ratios are independent of which mechanism (1)-(3) is assumed. For example, just by counting the extra quark spectators one predicts $(pp \to K^- X)/(pp \to K^+ X) \sim (1-x_K)^4$ and $(pp \to \bar{\Lambda} X)/(pp \to \Lambda X) \sim (1-x_L)^8$ which appears to be not inconsistent with experiment.[18] One also can predict ratios for different beams for massive lepton pair and ψ production. These and other applications are discussed in Ref. 19.

If the quark exchange or annihilation mechanism (3) is actually correct then there can be a remarkable, long-range correlation set up in double-fragmentation reactions. For example in $pp \to \pi^+_{(1)} \pi^+_{(2)} X$, with fast pions in the forward and backward direction, the requirement of quark exchange or $q\bar{q}$ annihilation forces an extra pair of spectators. One then predicts $d\sigma/dx_1\, dx_2\, (pp \to \pi^+_{(1)} \pi^+_{(2)} X) \sim (1-x_1)^3 (1-x_2)^7 + (x_1 \leftrightarrow x_2)$. This feature of the model and further examples are discussed in detail in a recent paper by Gunion and myself.[19]

V. How to See a Gluon Jet

Thus far in this talk, the emphasis has been on quark and multiquark jets. It is apparent that at some level QCD must imply the existence of gluon jets. Several essentially scale-invariant processes have been suggested to find such systems. For example, the subprocess $e^+e^- \to q\bar{q}g$ (see Fig. 15c') leads to a coplanar three-jet configuration,[22] and the reaction $\gamma^* q \to gq$ leads to a double jet structure in the current fragmentation region of deep inelastic electroproduction.[23] However, the background from constituent interchange model processes such as $e^+e^- \to q\bar{q}M$ and $\gamma^* q \to Mq$ is severe until very large p_T and $\sqrt{s}$; this is discussed in detail by DeGrand, Ng, and Tye.[24] Gluon jets, of course, may also be predicted in high p_T reactions from $gg \to gg$, $Mq \to gq$, etc.[25,26]

Recently Caswell, Horgan, and I[26] have considered several processes which must have a lower limit for gluon jet production if $\alpha_s \neq 0$. For example, by comparing contributions the subprocesses $q\bar{q} \to \gamma^* \to \mu^+\mu^-$ for large p_T single muons and $q\bar{q} \to \gamma g$ for large p_T (real or virtual) photons, we can derive a lower bound for scale-invariant hard photon production (see Fig. 13),[26]

$$\frac{E d\sigma/d^3p\,(pp \to \gamma X)}{E d\sigma/d^3p\,(pp \to \mu^+ X)} = \frac{\frac{4}{3}\alpha_s}{\alpha} \frac{4}{\langle \sin^2 \hat{\theta} \rangle} \tag{4.1}$$

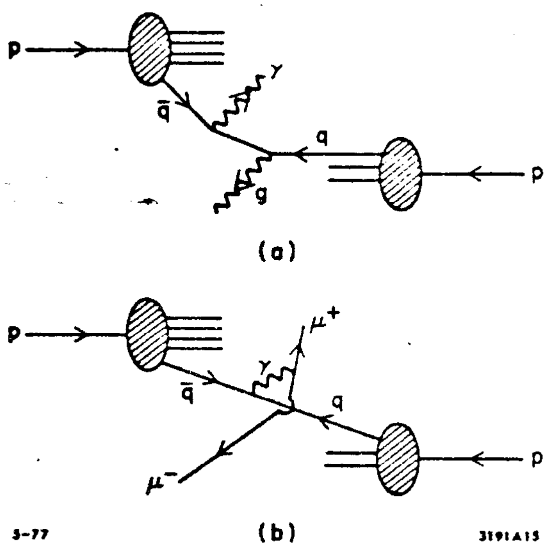

Fig. 13. (a) Contribution of the $q\bar{q}\to\mu^+\mu^-$ subprocess to μ^+ production at large p_T. (b) Contribution of $q\bar{q}\to\gamma g$ to real or virtual photon production at large p_T.

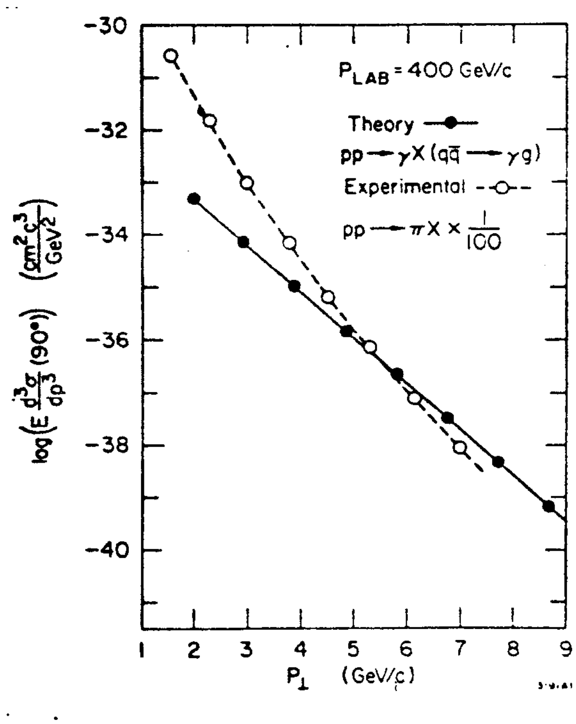

Fig. 14. Predicted contribution $Ed\sigma/d^3p$ $(pp\to\gamma X)$ at $p_{lab}=400$ GeV/c, $\theta_{c.m.}=90^0$ from the scale-invariant subprocess $(q\bar{q}\to\gamma g)$. For reference, the Chicago-Princeton data of Cronin et al. for $pp\to\pi X$ is shown multiplied by a vector meson dominant factor of 10^{-2}. From Ref. 26.

where $\hat{\theta}$ is the c.m. angle of the subprocess. This result should be applicable for $p_T \gtrsim 4$ GeV, where the $q\bar{q}\to\mu^+\mu^-$ subprocess dominates the single muon cross section. Notice that all the uncertainties from the q and $\bar{q}$ distributions cancel in this ratio. The predicted cross section for $\alpha_s=0.25$ and an estimated background from vector dominance terms are shown in Fig. 14. When the subprocess $q\bar{q}\to\gamma g$ dominates, a gluon jet is predicted on the away side of the direct photon, although other subprocesses such as $qg\to q\gamma$ can also contribute here.

In general, any collision that produces direct (real or virtual) hard photons, e.g., $pp\to\gamma+X$, $e^+e^-\to\gamma+X$, $ep\to e\gamma+X$, etc., will also produce a gluon jet with a cross section from the substitution $\alpha\to\frac{4}{3}\alpha_s$.[26] A useful way to verify the hard photon-quark current coupling in $e^+e^-\to q\bar{q}\gamma$ and $eq\to e\gamma q$ is to measure the charge asymmetry in $e^+e^-\to\gamma h^\pm X$, and $e^\pm p\to e^\pm\gamma X$ as discussed in Ref. 27.

A gluon jet may be identified from the global neutral character of its quantum numbers, and relative to quarks, the suppression of leading fragments. For example, one expects $G_{\pi/q}(x)/G_{\pi/g}(x)\sim\alpha_s(1-x)\log s/mq^2$ where the nonscaling factor is due to the dk_T^2/k_T^2 falloff of the $q\bar{q}g$ coupling. However, the most important discriminant of a gluon jet may be its hadron multiplicity density dn/dy in the central rapidity region. We discuss this possibility in the next sections.

VI. The Dynamics of Color Separation

One of the central questions in the quark-gluon description of hadron dynamics is the question of what controls the magnitude and energy dependence of hadron production. In a recent paper, Gunion and I[12] considered the possibility that the multiplicity distribution at high energies depends in a quantitative way on the color separation initially set up in the collision. In quantum electrodynamics, soft photons arise via bremsstrahlung from initial or final charged lines, and the average multiplicity is computed from the sum over all charged-particle pairs, each contribution depending on the product of their charges and a function which increases with the relative rapidity separation of the pair. In the analogous case of quantum chromodynamics, charge is replaced by color, and the hadrons—which are color singlets—do not radiate. Radiation of colored gluons occurs only when two colored objects (e.g., virtual quarks) are separated in rapidity. In addition there is a natural infrared cutoff determined by the size of the confinement region of color. We presume that the radiated color gluons eventually materialize as hadrons in such a way that the hadron multiplicity is a direct, monotonic function of the rising gluon multiplicity and hence only depends on the separating color currents. (A model where this relationship is linear is discussed in Section III.) Two processes with the same initial color-current configuration will thus produce the same multiplicity in the central rapidity region. (The principal effect of quark flavor will be to influence the quantum numbers of the leading hadrons.) The separation of color together with the eventual confinement of color thus leads naturally to a rising hadron multiplicity.

In the canonical case, $e^+e^- \to$ hadrons, the electromagnetic current produces at time = 0 a quark-antiquark pair, and there is an initial separation of color 3 and $\bar{3}$. Eventually the systems are neutralized and produce hadron jets, as in the model described in Section III. It is evident from the structure of QCD that the gluon radiation depends on the magnitude of the color charge and the rapidity separation of the q and $\bar{q}$ systems, and that it is flavor-independent; i.e., for the same rapidity separation the central hadron multiplicity is independent of which flavor quark pair is produced. In particular, we expect a decrease of $\langle n_{had}\rangle$ in $e^+e^- \to$ hadron at the charm (or other heavy quark) threshold, but otherwise $\langle n\rangle_{e^+e^- \to had} = n_{3\bar{3}}(s)$ will have a smooth monotonic increase with log s.

This simple connection of color separation to hadron production implies that the same function $n_{3\bar{3}}(s)$ controls the central region multiplicity in every process which begins with 3-$\bar{3}$ separation, e.g., deep inelastic lepton scattering $\ell p \to \ell' X$ ($\ell q \to \ell q'$), and the Drell-Yan process $A+B \to \ell\bar{\ell}X$ ($q\bar{q} \to \ell\bar{\ell}$). See Fig. 15a,b,c. However, if a collision involves the separation of other color charges, e.g., color octet jets produced from initial gluon exchange or production of a gluon jet, then we predict a different, higher, rapidity height. There is also the intriguing possibility of color interference when several color systems are separated.

A crucial question in the above analysis is how to interpret the spectator system when a wee quark is removed from the hadron wavefunction. We shall assume that Fock space quarks tend to have similar velocities and rapidities in a bound state, and thus at the time of the interaction the spectator system can be regarded as a coherent $\bar{3}$ state with the rapidity of the initial hadron.[12] On the other hand, if one assumes that the wee quarks are the children of gluons in lowest order perturbation theory,[9] then the spectator system would consist of a color octet at the rapidity of the hadron, and a $\bar{3}$ at the rapidity of the struck quark. This argument seems tenuous, though, since the quark partons can exchange gluons over the indefinite time before the interaction. The role of gluon exchange in electroproduction is discussed further in the next section.

Given the simple $\bar{3}$ structure of the spectator wavefunction, we then are led to universal multiplicity plateaus in the current and hadron fragmentation regions of deep inelastic scattering, and the prediction that the multiplicity in $\gamma^* p \to X$ is independent of q^2 at fixed $s=(q+p)^2$—even for real photons. These results[12] are in apparent agreement with experiment.[1]

It is perhaps useful to briefly review the multiplicity calculations for QED.[28] The analogous problem to the color situation is the calculation to all orders in α of the number of soft photons emitted by the outgoing muons in $e^+e^- \to \mu^+\mu^-$. The multiplicity is given by a Poisson distribution where $\langle n_\gamma\rangle$ is determined simply by lowest order matrix expression

$$\langle n_\gamma \rangle = -\frac{e^2}{(2\pi)^3} \int_{k_{min}}^{k_{max}} \frac{d^3k}{2k} \left(\frac{p_+^\nu}{p_+ \cdot k} - \frac{p_-^\nu}{p_- \cdot k} \right)^2$$

$$= \frac{\alpha}{2\pi} \left[\frac{1}{\beta} \log \frac{1+\beta}{1-\beta} - 2 \right] \int_{k_{min}}^{k_{max}} \frac{dk}{k} \tag{6.1}$$

Here $\beta = \left[1 - m^4/(p_+ \cdot p_-)^2 \right]^{1/2}$ is the relative velocity of the pair and $y = \frac{1}{2} \log \frac{1+\beta}{1-\beta}$ is the relative rapidity. A rapidity plateau arises naturally from the $k \cdot p$ singularity of the angular integration near the light cone, and the dk/k integration serves to modify the height of the plateau. In QED, $k_{min} = 0$, and $\langle n_\gamma \rangle$ is logarithmically infinite. In QCD where there is eventual confinement, the gluons of very long wavelength (k_{min} less than some hadronic size R^{-1}) decouple since they only see an overall color singlet system and the multiplicity can be finite. Since $k_{max} \lesssim \sqrt{s}/\langle n_\gamma \rangle$, we then have

$$\langle n_\gamma \rangle = \frac{2\alpha}{\pi} \left(\log \frac{s}{m^2} - 1 \right) \log \frac{k_{max}}{k_{min}} \qquad (s \gg m^2)$$

$$\cong \frac{\alpha}{\pi} \log \frac{s}{m^2} \log \frac{s}{k_{min}^2} \tag{6.2}$$

where the hadronic k_{min}^{-1} is the size of the color separation region. (In the model we discussed in Section III this region grows in proportion to $\sqrt{s}$.)

The result that the QED multiplicity (for $k_{min} \neq 0$) behaves as $\log^2 s$ at high energies is somewhat surprising and perhaps deserves further comment. We first emphasize that this contribution is not dominated by the photons produced at large k_T relative to the charged lines.[29] Even if we were to impose a cutoff at $k_T = k \sin\theta = k^{max}$, the angular integral still yields logarithmic form $\int d\theta^2/(\theta^2 + m^2/s) \sim \log s$. The actual transverse momentum distribution of the photons is interesting: the infinite sum in α falls off as a Gaussian[30] for moderate k_T^γ whereas at high k_T, the scale-invariant dk_T^2/k_T^2 hard photon perturbation theory component takes over. Furthermore, the single photon distribution has a hint of the "seagull" effect. If we use light cone variables with $x = (k_0 + k_3)/(p_0^+ + p_3^+)$,

$y = \log x + C$ then the leading $p_+ \cdot p_-$ term in Eq. (6.1) gives

$$\frac{dN}{d\vec{k}_T^2 \, dx} = \frac{\alpha/\pi}{k_T^2 + x^2 m^2} \, \frac{1}{\left[1 + \vec{k}_T^2 m^2/(2xp_+ \cdot p_-)^2\right]} \tag{6.3}$$

Thus $\langle \vec{k}_T^2 \rangle$ grows with $x^2 m^2$ at small $\vec{k}_T^2$. Notice that in the central region (e.g., $x \sim 0 (m/\sqrt{s})$), the rapidity distribution is essentially flat, with $dN/dy \sim \alpha/\pi \log s/k^2_{T\,\min}$.

Chromodynamics is of course much more subtle and complicated than electrodynamics, and all we shall do here is argue that QED at least provides a covariant and consistent model for multiparticle production which may represent a pattern for gauge theories. We also note that the work of Ref. 31 suggests the possibility that the radiation of gluons in QCD may exponentiate into an effective Poisson form when gluons of the same order in the quark current are properly grouped together.

VII. A Two Component Color Model

An intriguing feature, evident from the perturbation theory structure of QCD, is that all reactions can be classified according to whether the initial interaction separates a 3 and $\bar{3}$ of color or separates octets of color. This is illustrated in Fig. 15 for (a) electroproduction, (b) massive muon pair production, (c) e^+e^- annihilation, (d) high p_T processes, and even (e) ordinary forward interactions. In each case only the initial interaction is shown; there is then subsequent gluon (and hadron) radiation which neutralizes the colored systems.

Using the color model[12] discussed in Section VI, we expect all of the reactions on the left side of Fig. 15 to have the identical plateau height dn/dy for rapidities in the central region between the separated 3 and $\bar{3}$ systems. In fact all of the jet parameters $\langle \vec{k}_T^2 \rangle$, quantum number distributions, etc. should be indistinguishable in this region. In contrast to this we shall argue that whenever color octets are separated, the plateau height in the central region connecting their rapidities will be $2\frac{1}{4}$ times as high: $dn_{88}/dy = 9/4 \; dn_{3\bar{3}}/dy$; the number $9/4$ $[=2/(1-n^{-2})$ in color SU(n)$]$ is derived from the lowest order perturbation graphs for gluon emission.[12] Roughly speaking, an octet has a color charge equal to 3/2 that of the triplet.

We can also give an intuitive argument which shows why octet separation leads to a rapidity height at least twice that of separating triplets.[32] Consider the gluon exchange

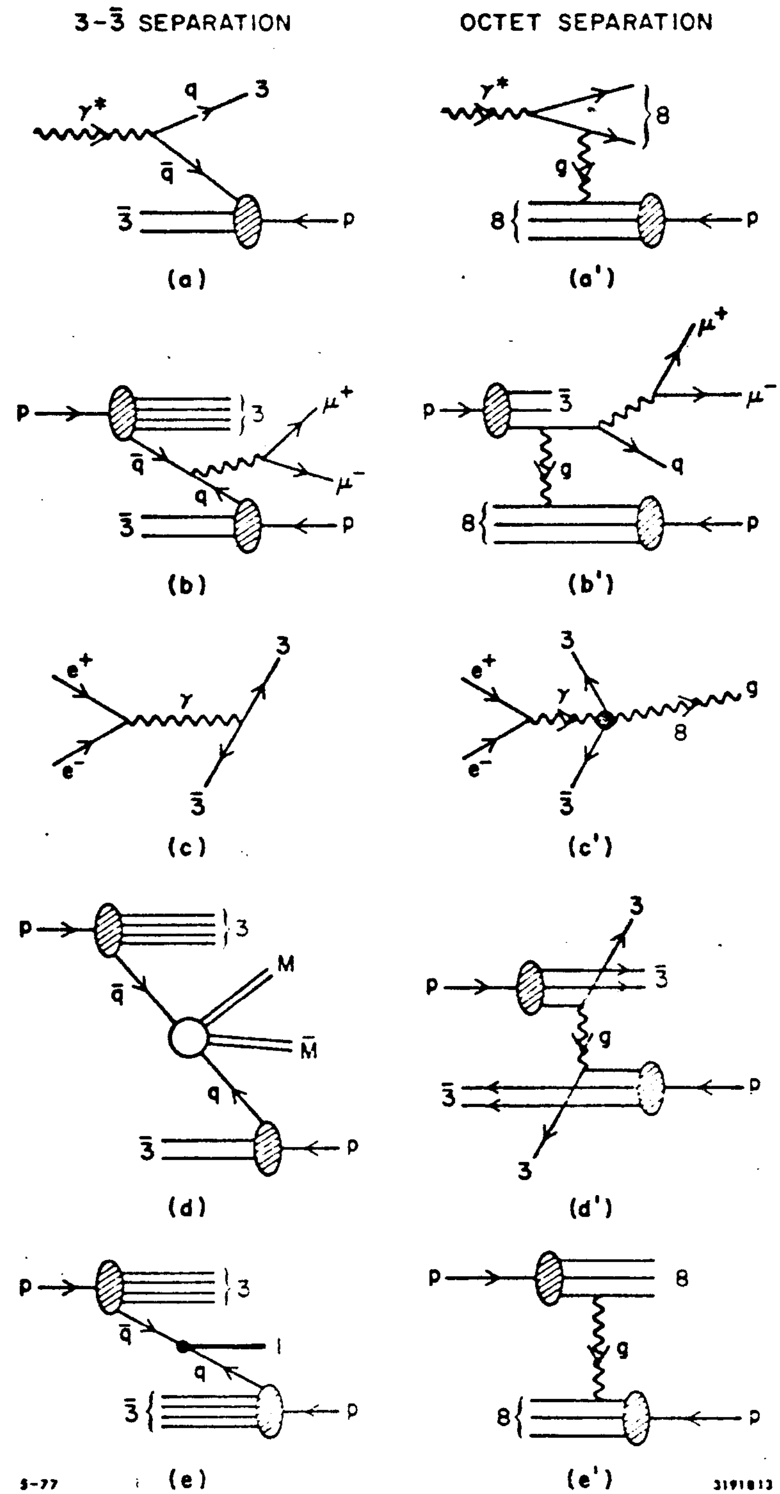

Fig. 15. Contributions to electroproduction, massive pair production, e^+e^- annihilation, large p_T hadron production, and forward hadronic collision, from both 3-$\bar{3}$ and octet-octet separation in color. In (e), the $q\bar{q}$ can annihilate to a color singlet or a wee quark can be exchanged.

diagram in Fig. 15d' for a large p_T reaction. It is clear that there must be two neutralization chains connecting the top and bottom 3 and $\bar{3}$'s, and the multiplicity will be double that of electroproduction at the corresponding kinematics for 3-$\bar{3}$ separation, as in Fig. 15a. At low p_T, the same graph reduces to the Low[20]-Nussinov[21] model for the Pomeron, Fig. 15e', and the two neutralization loops will interfere. The interference is not destructive since that would correspond to color singlet exchange. Thus the resulting multiplicity plateau height must be at least double that of electroproduction or $e^+e^- \to q\bar{q}$. The QED analogue of this result would be positronium + positronium $\to e^+e^-e^+e^-$ via photon exchange. For a high p_T collision the soft photon radiation has the usual plateau height along each outgoing lepton. At small p_T the interference of the radiation from different charged lines causes the plateau height to vanish in the case of photon exchange, but gives four times the height if the photon could transfer two units of charge. Notice that in the case of the color, the interference effect vanishes if $n_{color} \to \infty$.

It is possible that all hadron processes have both triplet- and octet-separation components, but that the latter is suppressed, at least at low energies, because of the extra associated multiplicity. Thus we speculate[12] that quark exchange and annihilation gives the dominant mechanism for massive pair production (Fig. 15b) (the Drell-Yan model) low multiplicity large p_T reactions (Fig. 15d) (the constituent interchange model), and by continuity to typical small p_T hadron reactions (wee quark exchange[4,12]). (See also the analysis of Section IV.) This ansatz, plus the color model, then can account for why the multiplicity plateau is observed to be essentially universal,[2] in all of these reactions.

On the other hand suppose we specifically consider events with high multiplicity, e.g., trigger only on events with at least double the usual hadron multiplicity. In this case the color octet diagrams on the right side of Fig. 15 will be favored, exposing the Berman, Bjorken, Kogut[33] gluon-exchange contribution for high p_T jets, and the Low-Nussinov gluon exchange mechanism for low p_T hadron reactions. Furthermore, a new essentially scale-invariant contribution from gluon exchange to $pp \to \mu^+\mu^- X$ shown in Fig. 15b' will be dominant. (Notice that, unlike the Drell-Yan mechanism, this contribution gives the same production cross section for proton and antiproton beams.)

Similarly, the double multiplicity trigger in $e^+e^- \to$ hadrons will enhance the $e^+e^- \to q\bar{q}g$ contribution.

A two component color model for ordinary forward reactions automatically leads to a correlation between left and right hemisphere multiplicities of the type observed at the ISR[34]: the gluon exchange component will be dominant for events with a large rapidity plateau height dn/dy are considered, thus giving a large multiplicity throughout the central region.

Finally, we emphasize that by studying events with at least double the average multiplicity in pp collisions, one may be able to study $qq \to qq$ scattering as it gradually evolves from the low p_T region (Fig. 15e') to high p_T scale-invariant jet production (Fig. 15d'). This can provide a nearly bias-free way of determining the jet-jet cross section.[35] Aside from its dependence on the effective coupling constant $\alpha_s(p_T)$ we emphasize that the gluon exchange term is scale-invariant, and thus unlike quark exchange, does not contain a strong p_T cutoff of the forward jets.

VIII. Conclusions

In this talk we have emphasized how the discrimination of various jet phenomena can determine the basic quark gluon mechanisms which control hadron dynamics. In particular, we have shown how quark, gluon, and multiquark jets can be distinguished by their retained quantum numbers, the leading-particle x dependence, and the multiplicity plateau height. A summary of representative jet parameters is given in Table I. Massive pair production reactions $A+B \to \ell^+\ell^- + X$ should be particularly interesting to study since the nature of the associated jets changes as one probes the wee and valence quark region. It is also interesting to study these quark and multiquark jet systems in a nuclear environment.

We have also emphasized the essential two-component nature of QCD and the relevant role of quark- and gluon-exchange mechanisms. In particular we have argued that wee quark exchange is the dominant hadron interaction at present energies. The ansatz that gluon exchange and production contributions can be made dominant by using a double multiplicity trigger could be an important phenomenological tool. Its confirmation would establish the dynamical role of color separation in multiparticle production.

Table I

Jet Type	Multiplicity	Example	Global Charge	Leading Particle	Typical Reactions
q	$n_{3\bar{3}}(s)$	u d	$\frac{2}{3} - \eta_Q$ $-\frac{1}{3} - \eta_Q$	π^+, $(1-x)$ π^-, $(1-x)$	current induced, large p_T, Drell-Yan
qq	$n_{3\bar{3}}(s)$	$(uu)_3$	$\frac{4}{3} + \eta_Q$	p, $(1-x)$ π^+, $(1-x)^3$	quark exchange reactions, Drell-Yan, baryon spectators
gluon	$n_{88}(s)$	g	0	M, $(1-x)^2 \log s$ B, $(1-x)^4 \log s$	$e^+e^- \to q\bar{q}g$, $pp \to \gamma X$, large p_T, current induced
B_8	$n_{88}(s)$	$(uud)_8$	1	p, $(1-x)$ π^+, $(1-x)^5$	gluon exchange in hadronic reactions, $B+B \to X$
M_8	$n_{88}(s)$	$(u\bar{d})_8$	1	π^+, $(1-x)$ p, $(1-x)^5$	gluon exchange in hadronic reactions, $M+B \to X$
B	constant	p	1	p, $(1-x)^{-1}$ Λ, $(1-x)$ π^+, $(1-x)^5$	diffractive dissociation
M	constant	π^+	1	π^+, $(1-x)^{-1}$ K^+, $(1-x)$	diffractive dissociation

References

1. For a review and references, see S. J. Brodsky and J. F. Gunion, Proc. VII International Colloquium on Multiparticle Reactions, Tutzing (1976).

2. The multiplicity data are summarized in E. Albini et al., Nuovo Cimento 32A, 101 (1976).

3. This section is based on work done in collaboration with N. Weiss. See S. J. Brodsky and N. Weiss, Stanford Linear Accelerator Center preprint SLAC-PUB-1926 (1977).

4. R. P. Feynman, Photon-Hadron Interactions (W. A. Benjamin, New York, 1972); Phys. Rev. Letters 23, 1415 (1969).

5. G. Farrar and J. Rosner, Phys. Rev. D 7, 2747 (1973). See also R. Cahn and E. Colglazier, Phys. Rev. D 9, 2658 (1974); J. L. Newmeyer and D. Sivers, Phys. Rev. D 9, 2592 (1974); D. Novseller, Phys. Rev. D 12, 2172 (1975).

6. R. D. Field and R. P. Feynman, Caltech preprint CALT-68-565 (1977).

7. J. Vander Velde, presented at the IV International Winter Meeting on Fundamental Physics, Salando, Spain (1976), University of Michigan preprint.

8. S. D. Drell and T.-M. Yan, Phys. Rev. Letters 25, 319 (1970).

9. V. A. Novikov, M. A. Shifman, A. I. Vainshtein, and V. I. Zakharov, preprint ITEP-112 (1976).

10. J. D. Bjorken, Proc. Summer Institute on Particle Physics, Stanford Linear Accelerator Center reports SLAC-167 and SLAC-PUB-1756 (1976). A. Casher, J. Kogut, and L. Susskind, Phys. Rev. Letters 31, 792 (1973).

11. R. Blankenbecler, S. J. Brodsky, and J. F. Gunion, Phys. Rev. D 12, 3469 (1975) and references therein.

12. S. J. Brodsky and J. F. Gunion, Phys. Rev. Letters 37, 402 (1976). I wish to thank T. DeGrand for discussions on color interference phenomena.

13. See also F. Low, XII Rencontre de Moriond (1977).

14. R. Blankenbecler and S. Brodsky, Phys. Rev. D 10, 2973 (1974). J. F. Gunion, Phys. Rev. D 10, 242 (1974). S. Brodsky and G. Farrar, Phys. Rev. Letters 31, 1153 (1973).

15. R. Blankenbecler and I. Schmidt, Stanford Linear Accelerator Center preprint SLAC-PUB-1881 (1977). See also S. Brodsky and B. Chertok, Phys. Rev. Letters 37, 269 (1976), and Phys. Rev. D 14, 3003 (1976).

16. R. Arnold et al., Phys. Rev. Letters 35, 776 (1975).

17. S. Brodsky and R. Blankenbecler, Ref. 14. See also H. Goldberg, Nucl. Phys. B44, 149 (1972).

18. J. C. Sens et al., quoted in W. Ochs, Nucl. Phys., to be published. F. E. Taylor et al., Phys. Rev. D 14, 1217 (1976). The $p \rightarrow \bar{\Lambda}/p \rightarrow \Lambda$ ratio on nuclei is consistent with $(1-x)^{8 \text{ or } 9}$. O. Overseth, private communication and W. Ochs, XII Rencontre de Moriond (1977).

19. S. Brodsky and J. Gunion, Ref. 1 (and to be published). See also W. Ochs, XII Rencontre de Moriond (1977).

20. F. Low, Ref. 13, and Phys. Rev. D 12, 163 (1975).

21. S. Nussinov, Phys. Rev. Letters 34, 1286 (1973). See also J. F. Gunion and D. E. Soper, UC-Davis preprint (1976).

22. J. Ellis, M. K. Gaillard, and G. C. Ross, Nucl. Phys. B111, 253 (1976).

23. E. G. Floratos, CERN preprint TH-2261 (1976).

24. T. De Grand, Y. J. Ng, and S.-H. H. Tye, to be published.

25. D. Sivers and R. Cutler, to be published.

26. S. J. Brodsky, W. Caswell, and R. Horgan, in preparation.

27. S. Brodsky, C. Carlson, and R. Suaya, Phys. Rev. D 14, 2264 (1976).
S. Brodsky, J. F. Gunion, and R. Jaffe, Phys. Rev. D 6, 2487 (1972).

28. D. R. Yennie, S. C. Frautshi, and H. Suura, Ann. Phys. 13, 379 (1961).

29. J. Dash, Marseille preprint (1977).

30. For a recent discussion, see G. Pancheri-Srivastava and Y. Srivastava, Northeastern University preprint (1976).

31. J. M. Cornwall and G. Tiktopoulos, UCLA preprints TEP 2 (1976) and TEP 10 (1976). J. C. Taylor et al., XVIII International Conference on High Energy Physics, Tblisi (1976) and J. Frenkel et al., Oxford preprint (1976).

32. Of course there is also the less interesting possibility that the result in QCD to all orders in perturbation theory (unlike QED) resembles thermodynamic models where the final state multiplicity has little to do with the initial process. I wish to thank J. Bjorken for conversations on this point.

33. S. Berman, J. Bjorken, and J. Kogut, Phys. Rev. D 4, 3788 (1971).
J. Bjorken, Phys. Rev. D 8, 3098 (1973).

34. See M. Benecke, XII Rencontre de Moriond (1977); and M. Benecke, A. Bialas, and S. Pokorski, Nucl. Phys. B110, 488 (1976). I wish to thank M. Benecke for discussions on this point.

35. For an alternative method, see W. Ochs and L. Stodolsky, XII Rencontre de Moriond (1977).

(B) LARGE TRANSVERSE MOMENTUM PROCESSES AND THE CONSTITUENT INTERCHANGE MODEL

(in collaboration with R. Blankenbecler and J. F. Gunion)

I. Introduction

Hadronic collisions involving the production of particles at large transverse momentum have the exciting potential of being able to resolve the underlying structure of hadrons and the interactions of their constituents at very short distances. The phenomenological features which have emerged from the recent ISR and Fermilab experiments—particularly the jet structure and the scaling laws of the inclusive cross sections—appear to be consistent with the properties expected from underlying two-body hard scattering subprocesses.[1-4] The data[4] for single particle cross sections, charge, momentum, and angular correlations are now so extensive that the constraints on models are overwhelmingly restrictive.

In this lecture we will present a comparison of this data with the predictions of the constituent interchange model[2] (CIM). The central postulate of the CIM is that the dominant short distance subprocesses are quark-hadron interactions (e.g., $qM \to qM$, $qB \to qB$, and the reactions related by crossing, $q\bar{q} \to MM$, etc.) which may be computed from an underlying scale-invariant field theory. We emphasize that such diagrams contribute in any quark model since their amplitude normalization is already fixed from the hadronic Bethe-Salpeter wavefunctions, elastic form factors, momentum sum rules for structure functions, etc. In fact, as we show in this paper, the CIM predictions are consistent not only with the scaling laws and angular dependence of the measured exclusive and inclusive large p_T cross sections, but also with their normalization. The new preliminary data from the British-French-Scandinavian group (BFS) presented at Flaine by Møller[5] on charge and momentum correlations also appear to support the basic features of the CIM subprocesses, in particular, the prediction of strong quantum number correlations between the trigger particles and the away side jet.

It should also be emphasized that dominance of the CIM diagrams at present energies is not incompatible with the assumption of a fundamental quark-gluon field theory such as quantum chromodynamics. In particular, the single gluon exchange term for quark-quark scattering,

$$\frac{d\sigma}{dt} = \frac{2}{9}\,\frac{4\pi\alpha_s^2}{t^2}\,\frac{s^2+u^2}{2s^2} \quad , \tag{1.1}$$

has been shown in Reference 6 to give a contribution below present data for $\frac{d\sigma}{d^3p/E}(pp \to \pi X)$ for all $p_T \lesssim 8$ GeV, assuming $\alpha_s\left(p_T^2\right) \lesssim .4$ (a conservative value). The CIM contributions will then dominate at lower p_T simply because of the relatively large effective hadron–quark coupling strengths. We note though that the $qq \to qq$ cross section could still be an important contribution to jet-trigger experiments in which the effect of trigger bias is removed.

II. CIM Predictions

In the constituent interchange model and other hard scattering models, the inclusive cross section for $A+B \to C+X$ at large p_T can be written as a convolution over structure functions $G_{a/A}(x_a, \vec{k}_{Ta})$, $G_{b/B}(x_b, \vec{k}_{Tb})$, and $G_{C/c}(x_C, \vec{k}_T^C)$ times the square of the matrix element for the subprocesses $a+b \to c+d$ (see Fig. 1). In a scale-invariant theory, dimensional counting[7] predicts at large p_T

$$\frac{d\sigma}{dt}(a+b \to c+d) \Rightarrow \frac{1}{\left(p_T^2\right)^{n_{active}-2}} f(\theta_{c.m.}) , \quad (2.1)$$

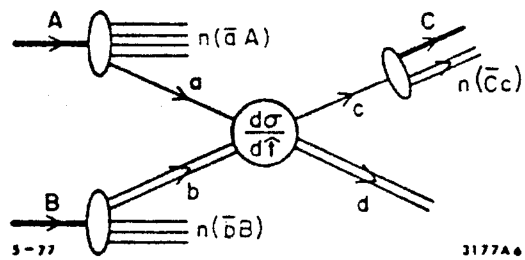

Fig. 1. Hard scattering subprocess contribution $ab \to c+d$ to the inclusive cross section $A+B \to C+X$.

where $n_{active} = n_a+n_b+n_c+n_d$ is the number of elementary fields in the subprocess, and[8] $G_{a/A}(x_a) \sim (1-x_a)^{2n(\bar{a}A)-1}$ at $x_a \to 1$, where $n(\bar{a}A)$ is the number of elementary particles left behind in the fragmentation of $A \to a$. These predictions are based on the short distance behavior of lowest order terms in renormalizable perturbation theories assuming a finite Bethe-Salpeter hadronic wave-function. Detailed discussions and comparisons with exclusive processes, form factors, large angle scattering, and structure functions are given in Refs. 4, 7, and 8.

The result of the convolution then gives the counting rules[7,8]

$$E\frac{d\sigma}{d^3p}(A+B \to C+X) = \sum_{abcd} \frac{1}{\left(p_T^2+m^2\right)^{n_{active}-2}} f(\epsilon, \theta_{c.m.})$$

$$\underset{\epsilon \to 0}{\sim} \sum_{abcd} \frac{1}{\left(p_T^2+m^2\right)^{n_{active}-2}} \epsilon^F f(\theta_{c.m.}) \quad (2.2)$$

where $\epsilon = \mathcal{M}^2/s = (1-x_T)$ at $\theta_{c.m.} = \pi/2$. Here n_{active} is the number of active fields in the high p_T subprocess (e.g., $n_{active} = 4$ for $qq \to qq$, 6 for $qM \to qM$) and $F = 2n_{spect} - 1$ where $n_{spect} = n(\bar{a}A) + n(\bar{b}B) + n(\bar{C}c)$ is the minimum number of elementary constituents that "waste" the momentum in the fragmentations $A \to a$, $B \to b$, $c \to C$ (e.g., $n_{spec} = 5$ and $F=9$ for $qq \to qq$ or $qM \to qM$ in $pp \to MX$). In general, one predicts that aside from normalization effects, the subprocesses with the minimum n_{active} (minimum p_T^{-1} power) and minimum n_{spect} (minimum F power) will dominate the cross section at large p_T, and small ϵ. Thus, given the fact that the $qq \to qq$ term has a small predicted normalization, the dominant terms for $pp \to \pi^{\pm}, K^+X$ will come from the $qM \to qM$ subprocess[2] (Fig. 2a):

$$\frac{d\sigma}{d^3p/E}(pp \to \pi^{\pm}, K^+, X) \sim \frac{\epsilon^9}{\left(p_T^2 + m^2\right)^4} f(\theta_{c.m.}) . \quad (2.3)$$

Here m^2 represents terms of order $\langle \vec{k}_T^2 \rangle$, m_q^2, etc. All other quark-hadron subprocesses lead to a higher power of $1/p_T$ or ϵ. In the case of K^- production, the dominant contribution at high p_T small ϵ will come from the "fusion" subprocess[3,2] $q\bar{q} \to K^- M$ (Fig. 2b)

$$\frac{d\sigma}{d^3p/E}(pp \to K^- X) \sim \frac{\epsilon^{11}}{\left(p_T^2 + m^2\right)^4} f(\theta_{c.m.}) . \quad (2.4)$$

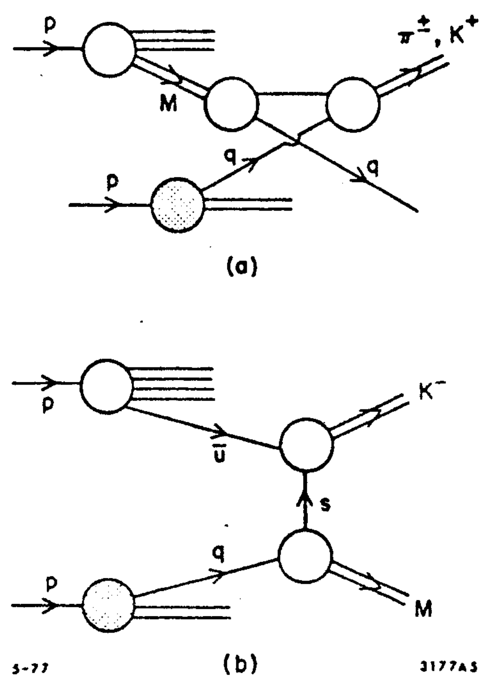

Fig. 2. Dominant CIM contribution to (a) $pp \to \pi^{\pm}$, K^+X and (b) $pp \to K^-X$.

A comparison of the CIM predictions with the experimentalists' fits to the Chicago-Princeton-Fermilab[9] data for $pp \to \pi^{\pm}, K^{\pm}, p^{\pm} X$ is shown in Table I. The agreement seems remarkable. For example, as shown in Fig. 3, the best fit for the Chicago-Princeton $\theta_{c.m.} = 90^{\circ}$ data for $pp \to \pi^+X$ is $p_T^{-8.2}(1-x_T)^{9.0}$ (with uncertainties in n and F order ± 0.5). The relative suppression of $E d\sigma/d^3p\,(pp \to \pi^- X)/E d\sigma/d^3p\,(pp \to \pi^+ X) \sim (1-x_T)$ evidently reflects the relative suppression of the d/u quark ratio in the proton structure function at large x.

Table I. Scaling predictions for $Ed\sigma/d^3p = C\,p_T^{-n}(1-x_T)^F$.

Large p_T Process	Leading CIM Subprocess	Predicted	Observed (CP)[9]
		n//F	n//F
$pp \to \pi^+ X$	$qM \to q\pi^+$	8//9	8.2//9.0
π^-	$qM \to q\pi^-$	8//9	8.5//9.9
K^+	$qM \to qK^+$	8//9	8.4//8.8
K^-	$q\bar{q} \to K^+K^-$	8//11	8.9//11.7
	$qM \to qK^-$	8//13	
$pp \to pX$	$q(qq) \to Mp$	12//5	11.7//6.8
	$qB \to qp$	12//7	
$pp \to \bar{p}X$	$q\bar{q} \to B\bar{p}$	12//11	(8.8//14.2)[a]
	$qM \to qM$	8//15	
	$M\bar{M} \to q\bar{q}$	8//15	
$\pi p \to \pi X$	$q\bar{q} \to M\pi$	8//5	
	$qM \to q\pi$	8//7	
	$q(qq) \to B\pi$	12//3	
	$\pi q \to \pi q$	8//3	

[a]The $\bar{p}$ fit has large uncertainties and is compatible with n=12, F=11.

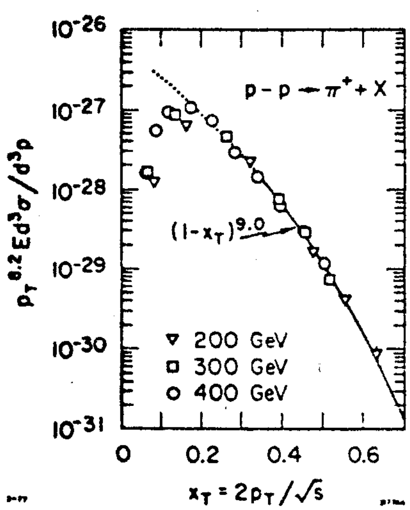

Fig. 3. Scaling law fit to the cross section $pp \to \pi^+ X$, $\theta_{c.m.} \cong 90^\circ$, $x_T = 2p_T/\sqrt{s} > 0.3$. From Ref. 9.

A crucial check on the identification of the underlying subprocess is the angular dependence of its cross section. The leading CIM contributions at high p_T to $pp \to \pi^+ X$ arise from the basic process

$$\frac{d\sigma}{d\hat{t}}(u\pi^+ \to u\pi^+) = \frac{C}{\hat{s}\hat{u}^3} \qquad (2.5)$$

and by $\hat{u} \to \hat{s}$ crossing

$$\frac{d\sigma}{d\hat{t}}(d\pi^+ \to d\pi^+) = \frac{C\hat{u}}{\hat{s}^5}\ , \qquad (2.6)$$

These predictions can be obtained by explicit calculation, or by using quark counting and the fact that the $u\pi^+ \to u\pi^+$ amplitude corresponds to spin 1/2 exchange in the u channel. It is easy to see that $d\pi^+ \to d\pi^+$ term gives a small contribution compared to the leading $1/\hat{s}\hat{u}^3$ term.

The angular dependence of the subprocess can be directly determined from experiment either from the correlated angular dependence of the away side jet[10] or the angular dependence of the $pp \to \pi X$ inclusive cross section.[11] In both cases the experimental p_T data are best fit with the form

$$\frac{d\sigma}{d\hat{t}} \propto \frac{1}{\hat{s}\hat{t}^3} \quad \text{or} \quad \frac{1}{\hat{s}\hat{u}^3} \tag{2.7}$$

(equivalent because of the pp symmetry). It should be emphasized that this angular dependence implies elementary spin 1/2 exchange in the t or u channel and is evidently difficult to reconcile with a subprocess based on quark-quark scattering.

The convolution of the distributions $G_{M/p} \sim (1-x)^5/x$, $G_{u/p} \sim (1-x)^3/x$ and the cross section for $uM \to u\pi^+$ gives the CIM prediction $Ed\sigma/d^3p\,(pp \to \pi^+) \propto p_T^{-8}\,\epsilon^9$, with the angular dependence given in Eq. (2.7). An immediate and important question is whether we can understand and predict the normalization of the cross sections as well. This will be discussed in detail in the next section. The CIM subprocesses also make detailed predictions for the quantum number flow of the valence quarks in large p_T reactions. We discuss this and the general question of jets and correlations in Section IV.

III. Normalization of CIM Subprocesses

A. The Meson-Quark-Antiquark Coupling

The magnitude of the amplitude $\mathcal{M}(u\pi^+ \to u\pi^+)$ required for the CIM predictions (see Fig. 2a) is directly related to the normalization of the Bethe-Salpeter vertex function for $\pi^+ \to u\bar{d}$ which in turn can be fixed by the normalization of the pion form factor or equivalently, the momentum sum rule for its structure function. The connection is clear from Fig. 4a-c. For simplicity we shall at first ignore the minor effects of spin and parametrize the large angle amplitude in Fig. 4a as $\mathcal{M}(u\pi^+ \to u\pi^+) = g^2/u$ where g represents the $\pi^+ \to \bar{u}d$ vertex function (i.e., coupling constant); g has dimensions of mass. Note that g refers to the effective coupling of the pion to its valence $q\bar{q}$ component, the wavefunction which dominates both the large angle elastic scattering amplitude and the meson structure function for x near 1.

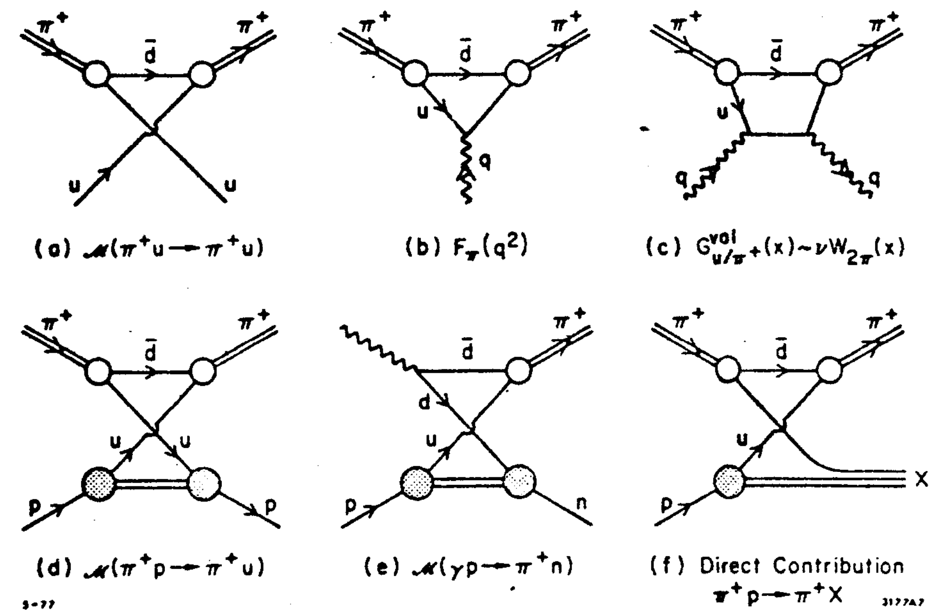

Fig. 4. Contribution of the $\pi^+u \to \pi^+u$ valence scattering amplitude (a), to the pion form factor (b), valence structure function (c), large angle $\pi^+p \to \pi^+p$ scattering (d), and inclusive scattering (f) (direct contribution). The relationship of photoproduction (e) to elastic scattering at large angles (c) is also shown.

The contribution of the valence state to the pion structure function is then

$$G^{val}_{u/\pi^+}(x) = \int d^2k_T \frac{g^2}{2(2\pi)^3} \frac{x(1-x)}{\left[\vec{k}_T^2 + M^2(x)\right]^2} \tag{3.1}$$

where $M^2(x) = m_u^2(1-x) + m_d^2(x) - x(1-x)m_\pi^2$, which we shall treat as a phenomenological constant. The fraction of the pion momentum carried by the valence quark in the pion is then

$$f^{val}_{u/\pi^+} \equiv \int_0^1 dx\, x\, G^{val}_{u/\pi}(x) = \frac{g^2}{4\pi}\frac{1}{4\pi}\frac{1}{\langle M^2(x)\rangle}\int_0^1 dx\, x^2(1-x) \tag{3.2}$$

A reasonable estimate is $\langle M^2(x)\rangle \sim .25\ \mathrm{GeV}^2$ (to set the mass scale of the pion form factor correctly) and $f^{val}_{u/\pi} \sim 0.05$ (from the empirical behavior of the fragmentation functions $D_{\pi^+/u}(x)$ at $x \gtrsim 0.8$ where $D_{\pi^+/u}(x) \sim G^{val}_{\pi^+/u}(x)$. This gives the rough estimate $g^2/4\pi \sim 1\text{-}2\ \mathrm{GeV}^2$. We note that more accurate information on $G_{\pi^+/u}(x)$ in the valence region could be obtained from forward pair production in the Drell-Yan process $\pi^+p \to \ell^+\ell^-X$. Note that g^2 includes the sum over color.

An important cross check to determine the coupling of the meson to its valence component is the magnitude of large angle meson-nucleon scattering and photoproduction.

Quark exchange diagrams such as those shown in Fig. 4d for π^+p scattering give an excellent parametrization of the fixed angle scaling behavior and angular dependence of the cross section $d\sigma/dt \propto s^{-1}t^{-4}u^{-3}$. A simple calculation, apparent from the impulse approximation structure of the diagrams, gives

$$\frac{d\sigma}{dt}(\pi^+p \to \pi^+p) \cong 4\,\frac{d\sigma}{dt}(\pi^+u \to \pi^+u)\; F_p^2(t)\left\langle \frac{1}{x^2} \right\rangle \tag{3.3}$$

(The factor of 4 comes from the two coherent diagrams. The $\pi^+d \to \pi^+d$ term is relatively small. The factors of x^{-1} occur here because the $\pi q \to \pi q$ amplitude is proportional to $(xu)^{-1} = \hat{u}^{-1}$ compared to the $eq \to eq$ coupling in $F_p(t)$ which is proportional to $\hat{x}s/t$.) Empirically, $d\sigma/dt \sim 0.4$ nb/GeV^4 at $t=u=-10$ GeV^2, giving $g^2/4\pi \sim 1.1$ GeV^2, taking $\langle x\rangle = 1/3$ (as expected from the proton valence wavefunction).

Alternatively we can consider the ratio of pion photoproduction $\gamma p \to \pi p$ and $\pi p \to \pi p$ scattering at fixed angle. The measured cross sections[13] are consistent with the dimensional counting predictions $d\sigma/dt \cong s^{-7} f(\theta_{c.m.})$ and $d\sigma/dt \cong s^{-8} f(\theta_{c.m.})$, respectively. In the CIM, the amplitudes only differ by the replacement of the direct photon coupling by the composite meson coupling, in Fig. 4e. Thus we have

$$\frac{\frac{d\sigma}{dt}(\gamma p \to \pi^+ n)}{\frac{d\sigma}{dt}(\pi^+p \to \pi^+p)} \cong \frac{2}{3}\,\frac{\bar{\lambda}^2\alpha}{g^2/4\pi}\,\langle x\rangle\, s \tag{3.4}$$

where $\bar{\lambda}^2$ is the average quark charge. Using the measured ratio[13] at $s = 10$ GeV^2, $\bar{\lambda}^2 = 5/9$, and $\langle x\rangle = 1/3$, we find $g^2/4\pi \sim 1.2$ GeV^2. Of all determinations of g^2 this invokes the least number of assumptions for parameter values, and thus should be the most reliable. We also note that the near equality of $d\sigma/dt\,(\pi^+p \to \pi^+p)$ and $d\sigma/dt\,(K^+p \to K^+p)$ at $\theta_{c.m.} = 90^\circ$, $s = 10$ GeV^2 implies that $g^2/4\pi$ is to first approximation SU(3) symmetric. We will discuss the implications of Eq. (3.4) for the inclusive γ/π ratio at high p_T in the next section. We can also predict the ratio of $d\sigma/dt\,(\gamma p \to \gamma p)$ to $d\sigma/dt\,(\gamma p \to \pi p)$ from a form similar to (3.4).

B. Normalization of Inclusive Reactions

Let us now try to predict the magnitude of inclusive large p_T reactions using the above coupling constant. The simplest contribution to $\pi p \to \pi X$ comes from the "direct" scattering graph, Fig. 4f. One only expects this "quasi-exclusive" diagram to be important at quite large $x_R = 1-\epsilon$ in analogy to the dominance of triple Regge contribution at large x_L. A simple estimate gives

$$\frac{d\sigma}{d^3p/E}(\pi p \to \pi X) \cong \frac{s}{\pi\left(m_X^2-t\right)}\ \nu W_2(x)\ \frac{d\sigma}{d\hat{t}}(\pi q \to \pi q) \quad ,$$

$$x = x_{bj} = -t/\left(m_X^2-t\right) \ , \tag{3.5}$$

where $d\sigma/d\hat{t}\,(\pi q \to \pi q)$ is evaluated at $\hat{s}=xs$, $\hat{u}=xu$, $\hat{t}=t$. The derived cross section behaves as $x_T(1-x_T)^3/p_T^8$. Using $g^2/4\pi = 1.2\,\mathrm{GeV}^2$, this direct contribution is in fact smaller than the observed cross section (but it should become dominant in $d\sigma/d^3p\,(\pi p \to \pi X)$ at $x_T \gtrsim 0.6$).

Let us now try to predict the cross section for $pp \to \pi X$ for the various contributing CIM subprocesses. For completeness, we give the general formula for the contribution of subprocesses each parametrized as

$$\frac{d\sigma}{d\hat{t}}(ab \to Cd) = \frac{\pi D}{s^{N-T-U}\,(-t)^T\,(-u)^U} \tag{3.6}$$

to the inclusive cross section for $A+B \to C+X$: $(\epsilon = 1-x_R,\ F = a+b+1)$

$$\frac{d\sigma}{d^3p/E}(A+B \to C+X) = \sum_{ab \to Cd} \frac{(1-x_R)^F}{\left(p_T^2\right)^N}(1+x_R z)^{-F^+}\ (1-x_R z)^{-F^-}\ I \ . \tag{3.7}$$

The coefficient is

$$I = Df_{a/A}\,f_{b/B}\,2^{F^+ + F^-}\ \frac{\Gamma(a+2)\,\Gamma(b+2)}{\Gamma(a+b+2)}\ J \tag{3.8}$$

where $J(z,\epsilon)$ is a slow function of $z = \cos\theta_{c.m.}$ and ϵ, and $J(z=0)=1$. Here $xG_{a/A} \sim (1-x)^a$, $xG_{b/B} \sim (1-x)^b$, $F^- = T+1+b-N$, and $F^+ = U+1+a-N$. Typically, processes involving a fragmentation or decay process $a+b \to c+d$ with $c \to C+X$ are relatively suppressed because of the higher p_T of the subprocess, and these will be neglected for the simple and rough estimates given here.

Thus let us consider the contribution of the subprocesses $Mq \to K^+q$ to $pp \to K^+X$, summing over the possible contributing meson states (see Fig. 2a). Here $d\sigma/dt = (g^4/16\pi)\,s^{-1}u^{-3}$, so $D = (g^2/4\pi)^2$, $N=4$, $T=0$, $U=3$. We take $G_{M/p}(x) \sim (1-x)^5$ and estimate $f_{M/p} \sim f_{\bar{q}/p}/f^{val}_{\bar{q}/\pi} \sim .03/.10 \sim .3$, $f_{q/p} \sim 0.3$ (only q=u makes a sizable contribution). Note that the f's are the fraction of momentum carried by both valence and non-valence states. The sum over mesons includes K^+, K^{+*}, K^o, K^{o*}, etc.; hence $\Sigma f_{M/p} \sim 4\, f_{M/p} \sim 1.2$.

If we take $g^2/4\pi = 1.2\ \mathrm{GeV}^2$, as determined from exclusive processes, then Eq. (3.7) gives at 90^o

$$\frac{d\sigma}{d^3p/E}(pp \to K^+X) \cong 1.9\, \frac{(1-x_R)^9}{p_T^8} \tag{3.9}$$

in GeV units. This is the prediction for the "prompt" K^+, those which are created directly in the subprocess. We estimate that the contribution from decays, etc., would multiply (3.9) by ~2 or 3. The Chicago-Princeton data[9] at $z = \cos\theta_{c.m.} = 0$ fits

$$\frac{d\sigma}{d^3p/E}(pp \to K^+X) \sim 5.1\, \frac{(1-x_R)^9}{p_T^8}\ . \tag{3.10}$$

After accounting for other subprocesses (e.g., $q\bar{q} \to K^+\bar{M}$), this seems satisfactory agreement. The fact that $E d\sigma/d^3p\,(pp \to \pi^+X)/E d\sigma/d^3p\,(pp \to K^+X) \sim 2.2$ in the data can be accounted for from extra resonance decay contributions for the pion and extra diagrams such as $\sim d\pi^+ \to d\pi^+$.

In the case of K^- production, the counting rules predict that the dominant contribution at large x_R should be the $q\bar{q} \to K^-M$ subprocess (Fig. 2b). By crossing we obtain (ignoring spin factors)

$$\frac{d\sigma}{dt}(q\bar{q} \to M\bar{M}) = (g^4/16\pi)\ \hat{t}/\hat{s}^2\hat{u}^3 \tag{3.11}$$

and a=3, b=7, F=11. Using (3.7) we obtain

$$E\frac{d\sigma}{d^3p}(pp \to K^-X) = (0.1\ \langle d\rangle)\ \frac{(1-x_R)^{11}}{p_T^8} \tag{3.12}$$

where $\langle d\rangle$ is the number of contributing recoil meson states. The data are consistent with

$$\frac{E d\sigma/d^3p\,(pp \to K^-X)}{E d\sigma/d^3p\,(pp \to K^+X)} \sim 0.9\ (1-x_R)^2 \tag{3.13}$$

so we require <d>$\sim$5 to 10 to completely account for this ratio (this is not an unreasonable estimate for the total number of contributing meson states). The subprocess $K^- q \to K^- q$ gives a $(1-x_R)^{13}/p_T^8$ contribution but its normalization is hard to estimate.

It should be emphasized that these calculations are only approximate due to uncertainties in the effects of spin, color, the small variation of J and the transverse momentum integrations. The main point here is that to within factors of 2 or 3 we find that the CIM diagrams immediately and simply account for the normalization of the inclusive cross section given the known non-zero coupling of the hadronic state to its valence quark components.

We can also proceed to calculate the normalization of the baryon subprocesses. From the magnitude of elastic pp scattering and the proton structure function sum rules, we find a coupling strength $h^2/4\pi \sim 30$ GeV^4 for the effective proton $\to$ q + (qq) coupling (where the (qq) system is at relatively low mass):

$$\frac{d\sigma}{d\hat{t}}(B+q \to B+q) \sim \frac{h^4}{16\pi^2}\,\frac{1}{\hat{s}^2\hat{t}^2\hat{u}^2} \tag{3.14}$$

The subprocess $B+q \to p+q$ then gives the contribution (z=0)

$$\frac{d\sigma}{d^3p/E}(pp \to pX) \sim 120\,\frac{(1-x_T)^7}{p_T^{12}}\quad, \tag{3.15}$$

where we have used the estimates $\Sigma f_{B/p} \sim 1.2$ and $\Sigma f_{q/p} \sim 0.5$. The CP data are consistent with this scaling behavior; the experimental coefficient is $\sim$170.

We must also consider the direct $pq \to pq$ contribution. In fact, using (3.7) we find this gives $E d\sigma/d^3p\,(pp \to pX) \sim 200\,(1-x_T)^3\, x_T^4/p_T^{12}$, and thus exceeds the contribution of (3.15) for $x_T \gtrsim 0.45$. It will be interesting to see if a change in the $(1-x_T)$ power from F=7 to F=3 is observed at the higher x_T values. There is also the possibility of an additional $p_T^{-8}\,(1-x_T)^7$ contribution from the subprocess $q+q \to B+\bar{q}$ but presumably the coupling constant for such large p_T processes is of order $(g^2/4\pi)^2$ and thus gives negligible contributions until considerably larger p_T values.

We have also computed the contribution of the fusion process $q\bar{q} \to B\bar{B}$ for $pp \to \bar{p}X$ production, using the crossed ($s \leftrightarrow t$) version of (3.14). This gives

$$\frac{E d\sigma/d^3p\,(pp \to \bar{p}X)}{E d\sigma/d^3p\,(pp \to pX)} \cong \frac{<d>}{10}\,(1-x_T)^4 \qquad (3.16)$$

where <d> is the number of opposite side baryon states. The value <d>~3-5 gives a consistent fit to experiment.

One can also work out in a similar way the various contributions to meson-induced processes. The subprocesses based on $Mq \to Mq$ are again predicted to dominate in the present x_T range and reasonable agreement is obtained with experiment. We also find that the formulae and normalizations are consistent with the exclusive-inclusive connection.

Finally, we note that we can readily predict the cross section for direct photon production simply by replacing the valence meson contribution in $Mq \to Mq$ by a photon to obtain $Mq \to \gamma q$. We predict

$$\frac{E d\sigma/d^3p\,(pp \to \gamma X)}{E d\sigma/d^3p\,(pp \to K^+X)} \sim \frac{2\alpha\lambda_q^2}{g^2/4\pi}\,p_T^2 \qquad (3.17)$$

at fixed x_T and $\theta_{c.m.}$. This gives $\gamma/\pi^0 \sim 0.005\, p_T^2$, or about 1/4 the value reported by Darriulat et al.[14] A similar estimate follows directly from the ratio of exclusive cross sections and crossing.

Finally, we note that our normalization estimate for the production of real photons can be extended to virtual photons, and it has been shown to agree with the data for massive lepton pair production in both its predicted magnitude and p_T dependence.[15]

IV. Correlations and High p_T Processes

One of the most important discriminants between models for high p_T production is the nature of the flow of the valence quantum numbers, momentum, and multiplicity produced in association with the high p_T trigger. The new preliminary ISR data from the British-French-Scandinavian group[5] gives a first look at the detailed effects associated with the quantum number of the trigger particle. The experiment utilizes the split field magnet facility combined with a wide angle spectrometer.

Figure 5 shows that the total momentum of charged particles on the same side and within one unit of rapidity y of the trigger particle (at $\theta_{c.m.} = 90^0$) increases very slowly with p_T for π^- and π^+ triggers, and not at all for K^-. In the CIM such behavior is expected since the trigger particle can be produced directly and alone in the subprocess or by low mass resonance decay. In models based on simple $qq \rightarrow qq$ scattering, extra momentum which scales with the trigger momentum is expected in the same side jet (although this effect could be reduced somewhat by transverse momentum fluctuations[11]). Furthermore, if the meson is produced as a fragment of a scattered valence u or d quark, then the greatest amount of same side momentum would have been expected in association with K^- than with K^+, π^+, or π^- triggers, just the opposite to what is seen!

A very dramatic feature of the preliminary BFS data is shown in Fig. 6. This shows the number of fast (p_T > 1.5 GeV/c) positive or negative particles per event in the away side jet ($|y| < 1$) opposite a $\pi^\pm$, $K^\pm$, or $p^\pm$ trigger at 90^0 with $3 < p_T^{trig} < 4.5$ GeV/c. One sees that there is significantly more fast positives than negatives opposite a K^- trigger, an effect not seen for π^-, π^+ and K^+ triggers. This is a direct indication that

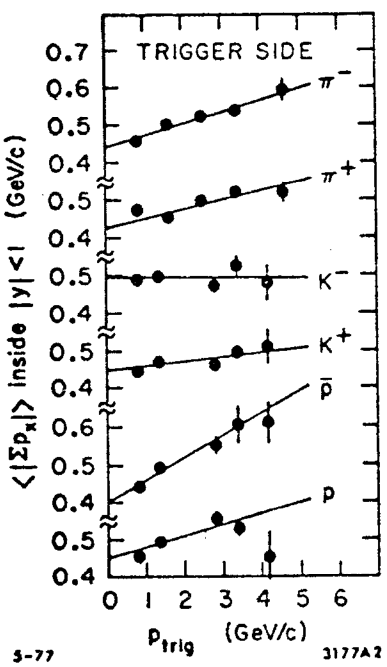

Fig. 5. The total momentum of particles along the 90^0 trigger particle for various charged particles. From Ref. 5.

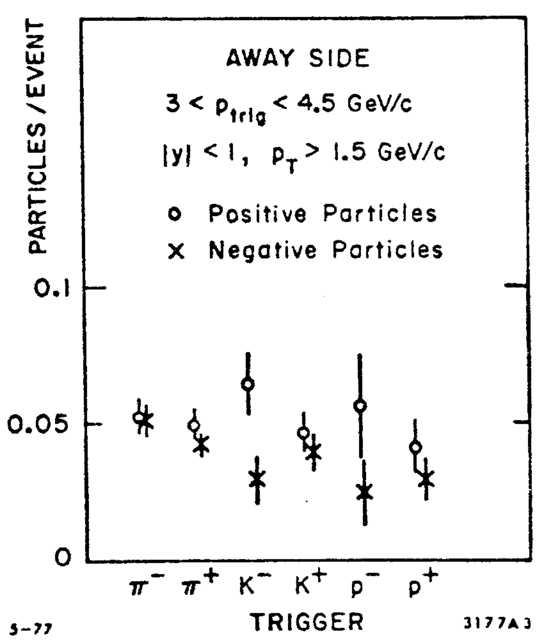

Fig. 6. Number of fast positive and negative particles on the side away from a 90^0 trigger for various trigger types. From Ref. 5.

there is a strong quantum number correlation between the trigger and away side jet. Such a correlation is not expected in a $qq \to qq$ model since the away side quark is not correlated in any obvious way to the trigger side quark: the away side jet should have quantum numbers completely independent of the trigger.

In the CIM, this charge correlation for the K^- trigger is a natural prediction of the model. In the case of $\pi^\pm$ or K^+ triggers the leading subprocess contribution is $qM \to qM$ scattering which produces an away side jet corresponding to u or d quark fragmentation. The average away charge is then[16].

$$\frac{1}{3}\left[2\left(\frac{2}{3} - n_Q\right) + \left(-\frac{1}{3} - n_Q\right)\right] = \frac{1}{3} - n_Q$$

where n_Q is the average charge of quarks in the sea (~0.07).[11,16] The $q\bar{q} \to M\bar{M}$ terms give additional contributions opposite in sign to the trigger charge. In the case of the K^- trigger, the dominant CIM subprocess is $q\bar{q} \to K^-M$ where M is either a positive or neutral strange mesonic system. The away side jet is thus predicted to have charge + 2/3 on the average. (In both cases this average charge estimate would increase slightly if we assume that $G_{u/p} > 2G_{d/p}$ at large x.) These predictions for the mean charge of the jet can be compared with the BFS data of Fig. 7 which shows the presence of a strong positively charged system in the jet recoiling against the K^- trigger with $p_{trig} > 2.5$ GeV.

One possible modification of the quark-quark scattering description would be to introduce a strong $q\bar{q} \to s\bar{s}$ quark-antiquark annihilation contribution specifically for K^- production. Although this would yield a quantum number correlation between the away and same side jets, the mean charge of the $\bar{s}$ system would not yield a sufficiently strong positive charge on the away side. In addition, the magnitude of the

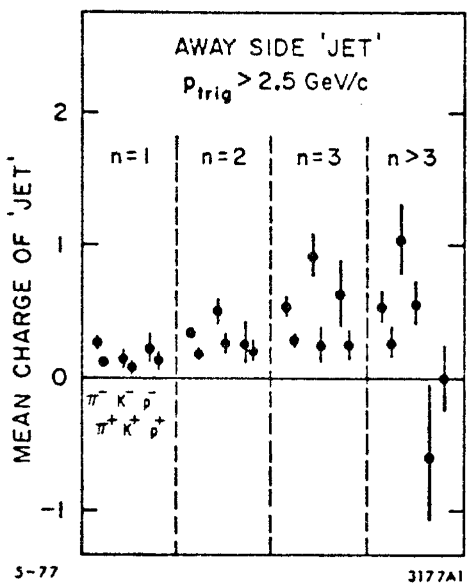

Fig. 7. Net mean charge of jet recoiling on the side away from the 90° trigger for various trigger types. See Ref. 5 for details of the definition of jet used here. (The data for $\bar{p}$ production is probably not statistically significant.) n is the number of charged particles seen in the jet.

$q\bar{q} \to s\bar{s}$ cross section is small if one crosses a form like $d\sigma/dt = s^{-1}t^{-3}$ for $qq \to qq$ to $q\bar{q} \to q\bar{q}$.

In general the distinctive quantum number flow of the CIM subprocesses can be used to predict a whole range of charge correlations associated with a high p_T trigger, corresponding to quark and multiquark jets in the fragmentation regions of the beam, target, or recoil jet. The quantum number retention[16] of these jets can also be tested in deep inelastic lepton scattering and the jets produced in the Drell-Yan process $A + B \to \ell^+\ell^-X$.

V. Jet Triggers and the CIM

Although the CIM appears to predict single particle data at large p_T very well, it is not clear that it can successfully account for the entire large jet trigger rate seen in the FNAL calorimeter experiment reported at this meeting.[17] The dominant jet-trigger contribution in the CIM comes from $Mq \to M'q$ subprocesses giving $d\sigma/d^3p_J/E_J \propto p_{TJ}^{-8}(1-x_{TJ})^9$. Since each meson in the pseudoscalar and vector SU(3) nonets contribute, and either the q or M system can provide the trigger, this gives a contribution at least 20 to 40 times the single meson rate at the same p_T. In addition there are contributions from other subprocesses $q\bar{q} \to M\bar{M}$, $M\bar{M} \to q\bar{q}$, $qB \to qB^*$, $q + qq \to M^* + B^*$, etc. which also provide jet triggers at high p_T. It may thus not be impossible to understand jet trigger cross sections which are 100 or more times larger than the single rate. However, one should also not rule out the possibility that because of the absence of the single-particle trigger bias, some jet trigger events could be due to QCD scale-invariant $qq \to qq$ scattering or processes involving gluon jets such as $gg \to gg$, $Mq \to gq$, etc. It will be crucial to have knowledge of the scaling behavior in p_T^J and x_T^J in order to begin to unravel these various contributions.

VI. Conclusions

As a summary it may be useful to contrast the basic assumptions and predictions of the CIM and quark-quark scattering models. The scaling laws of the CIM assume a basic scale-free theory, modulo logarithmic corrections characteristic of renormalizable perturbation theories.[18] Given that α_s is numerically small, the leading subprocess for $pp \to \pi^\pm$, $K^+ + X$ in the FNAL and ISR s, p_T range is then $qM \to qM$. The calculated subprocess cross section is $d\sigma/dt\,(qM \to qM) = \pi D/\hat{s}\,\hat{u}^3$ where the constant $D = (g^2/4\pi)^2$ is determined by the valence meson wavefunction normalization (see Section III). This form then correctly predicts the p_T, $\theta_{c.m.}$, x_T, and yields the normalization of the inclusive cross section.

In the approach of Feynman and Field,[17] Hwa et al.,[19] and others[20] sufficient scale-breaking is assumed so that literal quark-quark scattering can be taken to represent the large p_T subprocess. The form $d\sigma/dt = C/s\,t^3$ or $C/s\,u^3$ is then found to be a best simple fit to the data. (It should be remarked, though, that such a form, which corresponds to elementary spin 1/2 exchange in the t or u channel, is not natural for elastic qq scattering.) Both the $qM \to qM$ and $qq \to qq$ subprocesses correctly predict the $\sim(1-x_T)^9$ behavior of the inclusive cross section at fixed x_T and $\theta_{c.m.}$. Also, each model can account for the π^+/π^- and K^-/K^+ x_T dependence. Such ratios tend to be model-independent because one must pick up the same number of non-valence quarks somewhere in the inclusive process independent of the subprocess.

In the case of $pp \to pX$, the CP data[9] show a dramatic change in the p_T power to p_T^{-12} at fixed x_T and $\theta_{c.m.}$ (see Table I). In the CIM this is a natural consequence of the dominance of the $Bq \to Bq$ subprocesses, whose normalization is determined from $pp \to pp$ elastic scattering. (The calculated normalization of $qq \to B\bar{q}$ and $q + qq \to M + B$ turns out to be small in the present kinematic regime.) The CIM also predicts the observed $(1-x_T)^7$ behavior. In contrast, the $qq \to qq$ models, as interpreted by Feynman and Field, would lead to a $p_T^{-8}\ (1-x_T)^{11}$ behavior. One must then invoke new contributions such as the direct $pq \to pq$ subprocess (which gives an incorrect $(1-x_T)^3$ behavior) or perhaps $q + (qq) \to q + (qq)$ scattering.[11] New assumptions must then be introduced in the quark scattering model in order to calculate such additional processes. It then becomes doubly mysterious why processes such as $qM \to qM$ should not be considered for meson production.

In the case of the $\pi p \to \pi X$ cross sections, the $qq \to qq$ Feynman-Field model gives an excellent fit to the cross section provided $\nu W_2 \propto xG_{q/\pi}(x)$ goes to a finite constant ~ 0.15 at $x=1$. This assumption can be directly tested by checking for a flat non-vanishing Drell-Yan massive pair production cross section $d\sigma/dm^2\,dx_L(\pi p \to \ell^+\ell^- X)$ in the forward region, $x_L \sim 1$. In the CIM, the $\pi p \to \pi X$ cross section is computed from the subprocesses

$Mq \to Mq$, $q\bar{q} \to M\bar{M}$, as well as direct $\pi q \to \pi q$ scattering and is consistent with the data.

The CIM has the advantage of simultaneously predicting large p_T exclusive processes as well as inclusive cross sections in form as well as normalization. In the CIM one makes a natural progression from the proton form factor to the Compton amplitude to meson photoproduction to meson-proton scattering to inclusive cross sections, i.e. each case utilizing the same basic quark-exchange mechanism (see Fig. 4). In the case of the $qq \to qq$ model, there is no corresponding theory of exclusive reactions. For example, if $d\sigma/dt\,(qq \to qq) \sim C/st^3$ as determined by Feynman and Field[11] with $C = 2.3\,\mathrm{b}\cdot\mathrm{GeV}^6$ then one might expect a contribution $d\sigma/dt\,(pp \to pp) \sim C/st^3 F_p^4(t)$. However, the predicted normalization is then four orders of magnitude smaller than experiment at $s = 20\ \mathrm{GeV}^2$, $\theta_{c.m.} = \pi/2$. The angular dependence is also incompatible with the data, and the amplitude does not cross properly to $p\bar{p} \to p\bar{p}$.

Both the CIM and $qq \to qq$ models share the general features of hard scattering models for jet production angular correlations, etc. The predictions are in fact often indistinguishable since the same subprocess form is used. However, as we have emphasized here, the new preliminary charge correlation measurements of the BFS group,[5] particularly the K^- trigger data, implies quantum number correlations between the trigger and away side systems. Although such correlations are natural features of the CIM approach, it is not natural in a $qq \to qq$ model.

Finally, we again note that the CIM approach is not incompatible with the eventual dominance of a $\alpha_s^2 p_T^{-4} (1-x_T)^9$ scaling term from QCD in the single particle production cross section at very high p_T, probably well beyond $p_T = 8$ GeV. This $qq \to qq$ scattering contribution could, however, still make a significant $p_T^{-4} (1-x_T^J)^7$ contribution to the jet trigger cross section as presently measured.

A final version of this work will be published elsewhere.

References

1. S. M. Berman, J. D. Bjorken, and J. B. Kogut, Phys. Rev. D 4, 3388 (1971). J. Bjorken, Phys. Rev. D 8, 3098 (1973).
2. R. Blankenbecler, S. J. Brodsky, and J. F. Gunion, Phys. Letters B39, 649 (1972); 42, 461 (1973); Phys. Rev. D 12, 3469 (1975).
3. P. V. Landshoff and J. C. Polkinghorne, Phys. Rev. D 10, 891 (1974).
4. Additional references and reviews are given in D. Sivers, S. J. Brodsky, and R. Blankenbecler, Phys. Reports 23 (1976); P. Darriulat, XVIIIth International Conference on High Energy Physics, Tbilisi (1976); S. J. Brodsky and J. F. Gunion, Stanford Linear Accelerator Center preprint SLAC-PUB-1806, op.cit.; S. D. Ellis and R. Stroynowski, Stanford Linear Accelerator Center preprint SLAC-PUB-1903 (1977). See also G. Preparata and M. Rossi, CERN preprint (1976).
5. R. Møller, XIIth Recontre de Moriond, Flaine (1977).
6. R. F. Cahalan, K. A. Geer, J. Kogut, and L. Susskind, Phys. Rev. D 11, 1199 (1975). R. Cutler and D. Sivers, Argonne preprint and erratum (1977).
7. S. J. Brodsky and G. Farrar, Phys. Rev. Letters 31, 1153 (1973); Phys. Rev. D 11, 1309 (1975). V. Matveev, R. Muradyan, and A. Tavkhelidze, Nuovo Cimento Letters 7, 719 (1973).
8. R. Blankenbecler and S. J. Brodsky, Phys. Rev. D 10, 2973 (1974); J. Gunion, ibid. 10, 242 (1974). Spin corrections are discussed in Sivers et al., Ref. 4.
9. J. W. Cronin et al., Phys. Rev. D 11, 3105 (1975). M. Shochet et al., XVIIIth International Conference on High Energy Physics, Tbilisi (1976). D. Antveasyan et al., Phys. Rev. Letters 38, 112 (1977). Uncertainties in the n and F values are of order ±0.5 for $pp \to \pi^{\pm}, K^+X$, but are much larger for K^- and $\bar{p}$.
10. N. Baier, J. Cleymans, K. Kinoshita, and B. Petersson, Nucl. Phys. B118, 139 (1977). N. Baier and B. Petersson, XII Recontre de Moriond (1977). J. Ranft, op. cit.
11. R. D. Field and R. P. Feynman, Caltech preprint CALT-68-565 (1977). G. C. Fox, Caltech preprint CALT-68-573 (1977). R. Field, XII Rencontre de Moriond (1977).

12. R. Blankenbecler, S. J. Brodsky, and J. F. Gunion (in preparation).

13. R. Anderson et al. find $d\sigma/dt(\gamma p \to \pi^o p) = s^{-7.3\pm0.4} f(\theta_{c.m.})$ at $\theta_{c.m.} = \pi/2$. Phys. Rev. Letters 30, 627 (1973).

14. P. Darriulat, Ref. 2. For earlier theoretical work see G. R. Farrar and S. C. Frautschi, Phys. Rev. Letters 36, 1017 (1976) and G. R. Farrar, Caltech preprint, CALT-68-576.

15. M. Duong-van, K. V. Vasavada, and R. Blankenbecler, Stanford Linear Accelerator Center preprint SLAC-PUB-1882 (February 1977), submitted to Phys. Rev.

16. For a recent discussion of charge retention in quark and multiquark jets and applications, see S. J. Brodsky and N. Weiss, Stanford Linear Accelerator Center preprint SLAC-PUB-1926 (1977).

17. R. Field, Ref. 11. C. Bromberg et al., Caltech preprint 68-590 (1977).

18. A check on scaling corrections is provided by the empirical Drell-Yan scaling behavior of the $pp \to \mu^+\mu^- X$ cross section. See M. Shochet, XII Rencontre de Moriond (1977).

19. R. C. Hwa, A. J. Speissbach, and M. J. Teper, Phys. Rev. Letters 36, 1418 (1977); R. Hwa, XII Rencontre de Moriond (1977).

20. E. Fischbach and G. Look, Purdue University preprints (1976, 1977). A. P. Contogouris and R. Gasket, McGill preprint (1976). See also E. Levin and M. Ryskin, Yad. Fiz. 18, 1108 (1973).

(C) HADRON PRODUCTION IN NUCLEAR COLLISIONS— A NEW PARTON MODEL APPROACH

(in collaboration with J. F. Gunion and J. H. Kühn)

Although the quark-parton model has been very successful in predicting the short distance behavior of hadronic interactions, the underlying mechanisms involved in the production of hadrons in ordinary high energy collisions have never been specified. In the case of particle production on nuclear targets, this fundamental uncertainty of the parton approach becomes amplified, and this has led to an extraordinary range of divergent predictions for even the most basic experimental parameters.[1] In this talk we present a new approach to this problem based on a straightforward application of parton model concepts. The resulting picture for nuclear collisions is very simple and in good agreement with experiment. It is based upon (1) the assumption that each inelastically excited nucleon in the nuclear target produces hadrons independently of the others, and (2) a specific hadronic collision model based on wee parton interactions[2] analogous to the Drell-Yan[3] pair production process.

We begin with a simple parton model description of hadron-hadron interactions. Each hadron has a Fock-space decomposition in terms of multiparton states. An interaction occurs via a collision of a parton in the beam (B) with a parton in the target (A). The cross section takes the typical Drell-Yan form[3,4]

$$\sigma_{BA} = \sum_{\substack{a\in A\\ b\in B}} \int_0^1 dx_a \int_0^1 dx_b G_{a/A}(x_a) G_{b/B}(x_b) \hat{\sigma}_{ab}(\hat{s}_{ab}) \tag{1}$$

where

$$x_b = (k_b^o + k_b^z)/(p_B^o + p_B^z)$$

and

$$x_a = (k_a^o - k_a^z)/(p_A^o - p_A^z)$$

are the light-cone fractions ($p_B^z > 0$, $p_A^z < 0$) of the beam and target, respectively, and

$$\hat{s}_{ab} = x_a x_b s + \frac{m_a^2 m_b^2}{x_a x_b s}$$

is the collision energy squared of the subprocess. (For simplicity we do not display the transverse momentum dependence.) Expression (1) is Lorentz-invariant for boosts along the beam (z) direction. We presume that $\hat{\sigma}_{ab}$ falls rapidly with increasing $\hat{s}_{ab}$, as would be typical of quark-parton exchange[2,5] or q-$\bar{q}$ annihilation processes,[6] and that each distribution G(x) has the Feynman[2] wee parton distribution $xG(x) \to C \neq 0$ at $x \to 0$. In this model $\sigma_{BA}(s) \propto \log s$, and the location in rapidity of the parton-parton collision $\hat{y}$ is distributed uniformly throughout the central region, where neither x_a nor x_b is forced into the finite x, power-law damped regions of G(x). In inelastic collisions, the partons in the beam materialize as hadrons for $\hat{y} \lesssim y < Y_B$, and those in the target materialize throughout the interval $Y_A < y \lesssim \hat{y}$. Note that real hadron production from the beam partons cannot extend much below $\hat{y}$ since this forces propagators off-shell where interactions are suppressed.

Turning to nuclear collisions, we shall assume that, aside from small binding corrections and Fermi motion effects, each nucleon in the nucleus independently develops its own parton distribution. Thus the partons of different nucleons interact with each other only minimally and do not shadow or coalesce with one another.[7] In a high energy collision the various wee partons of the projectile can interact with the wee partons of different nucleons. The rapidity locations of the parton-parton collisions $\hat{y}_i$ are uncorrelated and uniformly distributed in the central region. Each nucleon in the nucleus A participates in only one interaction, whereas the mean number of inelastic collisions of the beam hadron H is $\bar{\nu} = A\sigma_{HN}^{inel}/\sigma_{HA}^{inel}$. On the average, then, the rapidity separation between parton collisions is $\Delta y \cong Y_c/(\bar{\nu}+1)$ where Y_c is the total length of the central rapidity region. A typical multiparticle distribution for $\bar{\nu} = 3$ collisions is illustrated in Fig. 1. Since the collision rapidities are uncorrelated, each inelastically excited nucleon produces hadronic multiplicity on the average halfway across the central region. As the number of collisions increases, the range of the projectile hadron distribution extends further and further into the central region to the minimum $\hat{y}_i$ —on the average over a rapidity length $\bar{\nu}\Delta y = (\bar{\nu}/(\bar{\nu}+1))Y_c$. Thus we immediately obtain for the ratio of multiplicities in the central region

$$\frac{\langle n\rangle_{HA}}{\langle n\rangle_{HN}} = \frac{\bar{\nu}}{2} + \frac{\bar{\nu}}{\bar{\nu}+1} \quad , \tag{2}$$

where the only dependence on the projectile H is through the definition of $\bar{\nu}$.

The distribution of particles averaged over events produced from the excitation of the nuclear partons is wedge-shaped. The ratio of distributions in the central region for hadron-nucleon to hadron-nucleus collisions is simply ($y_A \equiv 0$)

$$R_A(y) = \frac{(dn/dy)_{HA}}{(dn/dy)_{HN}} = \bar{\nu}\left(1 - \frac{y}{Y_c}\right) + \left[1 - \left(1 - \frac{y}{Y_c}\right)^{\bar{\nu}}\right]. \tag{3}$$

Although Eqs. (2) and (3) are derived assuming a uniform plateau height in the central region, corrections to this shape tend to cancel in the ratio.

Thus far we have ignored the effects of the fragmentation regions. Eq. (1) predicts that the fast (e.g., valence) partons interact only weakly[8] and thus $R_A(y) = 1$ in the projectile fragmentation region, and $R_A(y) = \bar{\nu}$ in the target fragmentation region. Let $\langle n_{frag}\rangle_H$ and $\langle n_{frag}\rangle_N$ be the average number of particles produced in the projectile and nucleon fragmentation regions (i.e., within $\Delta y_{frag} \sim 2$ units of the incident rapidity). Then, instead of Eq. (2), we obtain

$$\frac{\langle n_{tot}\rangle_{HA}}{\langle n_{tot}\rangle_{HN}} = \frac{\left(\frac{\bar{\nu}}{2}+\frac{\bar{\nu}}{\bar{\nu}+1}\right)\langle n_{central}\rangle + \bar{\nu}\langle n_{frag}\rangle_N + \langle n_{frag}\rangle_H}{\langle n_{tot}\rangle_{HN}}$$

$$= \left(\frac{\bar{\nu}}{2}+\frac{\bar{\nu}}{\bar{\nu}+1}\right) - \left(\frac{\bar{\nu}}{2}-\frac{1}{\bar{\nu}+1}\right)\frac{\langle n_{frag}\rangle_H}{\langle n_{tot}\rangle_{HN}} + \left(\frac{\bar{\nu}}{2}-\frac{\bar{\nu}}{\bar{\nu}+1}\right)\frac{\langle n_{frag}\rangle_N}{\langle n_{tot}\rangle_{HN}}, \qquad (4)$$

where $\langle n_{tot}\rangle_{HN} = \langle n_{central}\rangle + \langle n_{frag}\rangle_N + \langle n_{frag}\rangle_H$ is the total produced multiplicity for the H-N collision. In practice the fragmentation correction terms are small, of order $(\Delta y)_{frag}/Y_{total} \sim O(1/\log s)$ compared to $\bar{\nu}/2$.

This result is compared with the data summary of Busza et al.[9] in Fig. 2 for $p_{lab} = 200$ GeV, taking $\langle n_{frag}\rangle_H/\langle n_{tot}\rangle \sim \langle n_{frag}\rangle_N/\langle n_{tot}\rangle \sim .2$. It is in good agreement with the data for charged pion and proton collisions. In addition, the shapes of the observed multiplicity distributions are consistent with the predicted forms of Eq. (3) and Fig. 1. The slight energy dependence predicted in Eq. (4) is also consistent with the trend of the data.[10]

We have analyzed the total nuclear cross section in this model and have found it to be consistent with the usual Glauber theory.[11] In this picture the incident hadron, which is represented by its Fock-space parton distribution, can interact elastically (diffractively) via elastic parton interactions in the central region and can continue to propagate and interact as a coherent hadron through the nuclear medium.[12] Thus one obtains the usual multiple-scattering Glauber series. Nonetheless, the multiplicity density dN/dy produced from the incident projectile parton distribution is not increased by the repeated collisions. Because of the Glauber series, the cross section of course does not factorize: $\sigma_{\pi A}^{inel} \sim \sigma_{pA}^{inel}$ approach the geometric limit.

The model proposed here is consistent with energy and momentum conservation. In the equal velocity frame, the central particles produced in the projectile direction have a typical total energy of order $\bar{\nu} m_T$, $(m_T^2 = m^2 + \langle \vec{k}_\perp^{\,2}\rangle)$,

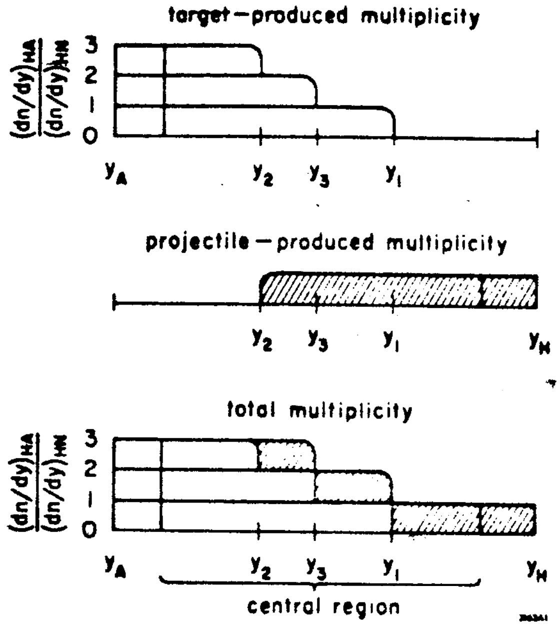

Fig. 1. Idealized multiplicity distribution for an H-A collision with $\bar{\nu}=3$ inelastic excitations. The y_i are uniformly distributed in rapidity and can be produced in any sequence. The central and fragmentation (s-independent) regions are indicated.

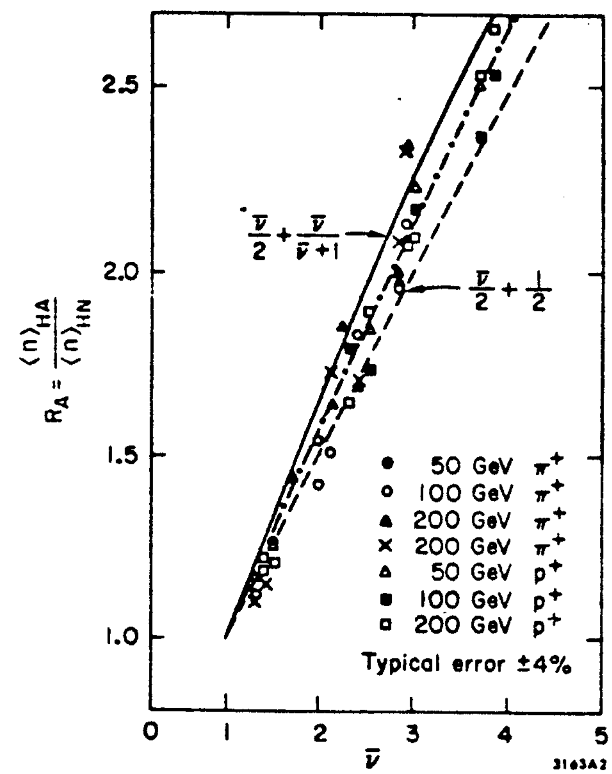

Fig. 2. The variation of $R_A = \langle n \rangle_{HA}/\langle n \rangle_{HN}$ with $\bar{\nu}$ for pion and proton beams. The data are for charged multiplicities from Ref. 1. The solid curve is the $s \to \infty$ prediction $R_A = \bar{\nu}/2 + \bar{\nu}/(\bar{\nu}+1)$. The dashed curve is the line $R_A = \bar{\nu}/2 + 1/2$ corresponding to no central region. The prediction of the model, Eq. (4), for $E_{lab} = 200$ GeV (taking $\langle n_{frag} \rangle_{H,N}/\langle n_{tot} \rangle = .2$) is the dashed-dotted curve, $R_A = \bar{\nu}/2 + \bar{\nu}(\bar{\nu}+1) - .2(\bar{\nu}-1)/(\bar{\nu}+1)$.

which can be compensated by a small loss of energy of the leading particles in the projectile region, a correction of relative order $\bar{\nu} m_T/\sqrt{s}$.

One may also use this picture to predict the multiplicity distributions in nucleus-nucleus collisions.[12] For the central region one obtains

$$\frac{\langle n\rangle_{A_1A_2}}{\langle n\rangle_{NN}} = \bar{\nu}_{A_1/A_2}\left(\frac{\bar{\nu}_{A_2/N}}{\bar{\nu}_{A_2/N}+1}\right) + \bar{\nu}_{A_2/A_1}\left(\frac{\bar{\nu}_{A_1/N}}{\bar{\nu}_{A_1/N}+1}\right), \tag{5}$$

where

$$\bar{\nu}_{A_1/A_2} = \frac{A_1\sigma_{NA_2}}{\sigma_{A_1A_2}}$$

is the average number of inelastically excited nucleons in A_1 in collision with a projectile A_2. Each such excited A_1 nucleon interacts inelastically with $\bar{\nu}_{A_2/N}$ nucleons in A_2 so that the average rapidity length of excited partons in A_1 is

$$\left[\bar{\nu}_{A_2/N}/\left(\bar{\nu}_{A_2/N}+1\right)\right] Y_c.$$

Corresponding statements apply to $\bar{\nu}_{A_2/A_1}$ and $\bar{\nu}_{A_1/N}$. The above result predicts, for example, $\langle n\rangle_{\alpha A_2}/\langle n\rangle_{NA_2} \sim 3.8$ for $A_2 > 100$, which is in agreement with cosmic ray data for alpha-particle collisions.[13]

Finally, we wish to point out the connection between our hypothesis of independently interacting and materializing nuclear parton chains and deep inelastic scattering measurements on nuclei. The latter directly probe the parton distributions within nuclei, and, according to our hypothesis, one should obtain

$$\nu W_{2A}(x_{Bj}) \cong A\nu W_2(x_{Bj}) \tag{6}$$

for all (including arbitrarily small) $x_{Bj} = -q^2/2M_N\nu \lesssim 1$ once q^2 is in the Bjorken scaling region.[14] For $x_{Bj} > 1$, Fermi motion corrections can be included and computed using quark counting,[15] but otherwise nuclear binding corrections to

(6) are considered negligible. Thus there is neither shadowing nor antishadowing[16] of the partons of one nucleon by the partons of other nucleons. In general, we predict the absence of shadowing — independent of beam energy — for any reaction where the effective collision energy of the subprocess is large, e.g., for the Drell-Yan Process $pA \to \ell^+\ell^- X$ at large $\mathcal{M}^2_{\ell^+\ell^-}$, as well as for large p_T hadronic reactions — ignoring multiple scattering effects.[17] The absence of shadowing is also apparent in the ratio of distributions $R_A(x) = (dn/dx)_{HA}/(dn/dx)_{HN}$ where x is the Feynman variable $k_{c.m.}/k^{max}_{c.m.}$. At infinite energy $R_A(x)$ reduces in our model to a step function $R_A(x) = \bar{\nu}\theta(-x) + \theta(x)$ since the central region is confined to $x \to 0$. If we identify the nuclear parton distribution shape with the multiparticle distribution for $x < 0$, this again corresponds to the absence of shadowing: $(d\sigma/dx)_{HA} = A(d\sigma/dx)_{HN}$.[18]

In summary, we have found that the parton model can be consistent with both the strong absorption of nuclear cross sections and the relatively low multiplicity of hadron-nucleus collisions. Another problem which could be analyzed in this model is the propagation of virtual quark states and unstable resonances through the nuclear medium.[19, 20]

Acknowledgements

In addition to my collaborators, I wish to thank X. Artru, M. Beneke, J. Bjorken, A. Capella, T. DeGrand, T. Jaroszewicz, A. Krzywicki, F. Low, H. Miettinen, W. Ochs, D. Sivers, and V. I. Zakharov for helpful conversations. I also wish to thank Professor S. Pokorski and his colleagues at Warsaw University for their kind hospitality at the Kazimierz Symposium.

References

1. For a review of the data and various theoretical models, see W. Busza, in Proc. VII Int. Colloquium on Multiparticle Reactions, Tutzing, Germany, 21-25 June 1976.

2. R. P. Feynman, Photon-Hadron Interactions (W. A. Benjamin, Inc., Reading, Mass., 1972) and references therein.

3. S. Drell and T. M. Yan, Phys. Rev. Lett. 25, 316 (1970) and Ann. Phys. (N.Y.) 66, 578 (1971).

4. A model of this form was considered by P. V. Landshoff and J. Polkinghorne, Nucl. Phys. B 32, 541 (1971).

5. R. Blankenbecler, S. J. Brodsky, and J. F. Gunion, Phys. Rev. D 8, 287 (1973), Phys. Rev. D 12, 3469 (1975), and references therein.

6. P. V. Landshoff and J. Polkinghorne, Phys. Rev. D 10, 891 (1974).

7. We emphasize that nuclear binding and Fermi-motion corrections are not related to the "$A^{2/3}$" surface or nuclear size effects characteristic of shadowing.

8. This was first discussed by O. Kancheli, JETP Lett. 18, 274 (1973).

9. W. Busza, P. Luckey, L. Votta, C. Young, C. Halliwell, and J. Elias, paper submitted to XVIII Int. Conf. on High Energy Physics, Tbilisi, USSR, 15-21 July 1976.

10. Recently, A. Capella and A. Krzywicki, Orsay preprint LPTHE 771? (1977), proposed an extended multiscattering model in which higher order Glauber terms correspond to the interaction of $n = 1, 2, \ldots$ independent constituent systems within the projectile, each of which shares the incident energy roughly equally, $\hat{s} \sim s/n$. At present energies their model also agrees well with experiment. However, the energy dependence of this model

differs from the model discussed here; e.g., the nuclear chains all extend to the projectile fragmentation region and $\langle n\rangle_{HA}/\langle n\rangle_{HN} \rightarrow \bar{\nu}$ at infinite energy. The effect of the multichains on the parton distribution of the projectile (νW_{2H}) must also be understood.

11. R. Glauber, in Lectures in Theoretical Physics, Vol. I, ed. W. E. Britten and G. Dunham (Interscience, New York, 1959). The generalized Glauber theory resulting from this model includes inelastic diffractive states which can be treated in the fashion of photon-hadron interactions, as in S. J. Brodsky and J. Pumplin, Phys. Rev. 182, 1794 (1969), and V. Gribov, JETP 30, 709 (1970). For a recent discussion and references for multi-scattering models see J. Weis, CERN preprint TH.2197 (1976). We are grateful for discussions with H. Miettinen and J. Weis on this subject.

12. Since the parton scattering is almost forward, the initial Fock-space state is disturbed only minimally. It thus has considerable overlap and remains nearly coherent with the incident projectile wave function. A complete discussion will be presented in S. J. Brodsky, J. F. Gunion, and J. Kühn, to be published.

13. The experimental ratio is ~ 4. See M. F. Kaplon and D. M. Ritson, Phys. Rev. 85, 932 (1952); Phys. Rev. 88, 386 (1952). We wish to thank D. Ritson for a discussion of these data. For other theoretical treatments see A. Bialas, M. Bleszynski, and W. Czyz, Nucl. Phys. B 111, 461 (1976) and references therein.

14. This possibility was suggested, for instance, in S. J. Brodsky, F. Close, and J. F. Gunion, Phys. Rev. D 6, 177 (1972). Note that this is contrary to the result predicted by Zakharov and Nicolaev (Ref. 16). See also J. D. Bjorken, Proc. SLAC Summer Institute, Stanford, California, 21-31 July 1975.

15. A. Krzywicki, Phys. Rev. D 14, 152 (1976). S. J. Brodsky and B. Chertok, Phys. Rev. D 14, 3003 (1976). I. A. Schmidt and R. Blankenbecler, Stanford Linear Accelerator Center preprint SLAC-PUB-1881 (1977).

16. V. I. Zakharov and N. N. Nikolaev, Phys. Lett. 55B, 397 (1975). N. N. Nikolaev, IV Int. Seminar on the Problems of High Energy Physics, Dubna, USSR, 1975, and Int. Seminar on Particle-Nuclear Interactions, ICTP, Trieste, Italy, 1976.

17. Multiple scattering effects are discussed by J. H. Kühn, Phys. Rev. D 13, 2948 (1976). Notice also that we predict that the multiplicity produced in the no-shadowing domain is that appropriate to just one "wounded" nucleon, modulo possible cascading.

18. These results are also consistent with the cutting rules of V. A. Abramovski, V. N. Gribov, and O. V. Kancheli, Sov. J. Nucl. Phys. 18, 308 (1974).

19. For a review of unstable resonance cross sections see G. Fäldt, Topical Meeting on Multiparticle Production on Nuclei at Very High Energy, Trieste, Italy, 10-15 June 1976.

20. Bjorken scaling of the virtual photoabsorption cross sections $\sigma_T(q^2, \nu) \propto (q^2)^{-1}$ at high ν and the scale-invariant behavior for $\sigma(e^+e^- \to \text{hadrons})$ at large s implies, in a generalized vector dominance model, that the diffractive cross section for virtual meson states $\sigma(\mathcal{M}^2, \nu)$ decreases at least as fast as $\mathcal{M}^{-2}$. See J. D. Bjorken (Ref. 14), S. Brodsky and J. Pumplin (Ref. 11), and V. N. Gribov (Ref. 11). Since the high mass states interact weakly, this again implies the absence of shadowing in deep inelastic lepton scattering, Eq. (6).